

# Physiological and Theoretical Analysis of $K^+$ Currents Controlling Discharge in Neonatal Rat Mesencephalic Trigeminal Neurons

CHRISTOPHER A. DEL NEGRO AND SCOTT H. CHANDLER

*Department of Physiological Science, University of California at Los Angeles, Los Angeles, California 90095-1568*

**Del Negro, Christopher A. and Scott H. Chandler.** Physiological and theoretical analysis of  $K^+$  currents controlling discharge in neonatal rat mesencephalic trigeminal neurons. *J. Neurophysiol.* 77: 537–553, 1997. Whole cell voltage- and current-clamp recordings were obtained from mesencephalic trigeminal sensory (Mes 5) neurons identified visually in thin brain stem slices of neonatal rats with the use of infrared video microscopy. These cells exhibited accommodation in spike discharge responses to depolarizing current injection protocols whose duration differed as a function of holding potential ( $-50$  vs.  $-65$  mV). Several spikes were elicited before the membrane response accommodated from  $-50$  mV, whereas from  $-65$  mV only single action potentials were evoked. In response to similar protocols, application of the  $K^+$  channel blocker 4-aminopyridine (4-AP) ( $50 \mu\text{M}$  to  $2$  mM) caused sustained repetitive spiking whereas tetraethylammonium (TEA) ( $10$ – $30$  mM) did not cause repetitive spiking. In voltage clamp, 4-AP application ( $100 \mu\text{M}$ ) revealed a sustained outward current ( $I_{4\text{-AP}}$ ) that was active between  $-60$  and  $-30$  mV.  $I_{4\text{-AP}}$  was responsible for suppressing sustained repetitive spiking behavior, producing accommodation under normal circumstances. TEA application in voltage clamp revealed a sustained outward current evoked positive to  $-40$  mV. Two transient outward currents (TOCs) were identified by prepulse protocols typically used to characterize A-type currents: a 4-AP-insensitive fast TOC, and a slow TOC ( $I_{\text{TOC-S}}$ ) sensitive to 4-AP ( $>500 \mu\text{M}$ ). A  $\text{Ca}^{2+}$ -dependent outward current that activated positive to  $-30$  mV was also characterized. A mathematical model of a Mes 5 neuron was assembled from our voltage-clamp records to simulate the dynamic interaction of outward currents during membrane excitation. We conclude that in Mes 5 neurons, the 4-AP-sensitive currents  $I_{\text{TOC-S}}$  and  $I_{4\text{-AP}}$  determine the duration of spike trains. In particular, the noninactivating  $I_{4\text{-AP}}$  determines whether cells exhibit sustained repetitive discharge or accommodate in response to depolarizing current. Neurotransmitter modulation of this current or modulation of the resting membrane potential could modify the output properties of Mes 5 neurons, and therefore the properties of these currents must be incorporated into our current understanding of how these cells contribute to shaping oral-motor pattern generation.

## INTRODUCTION

Neuronal mechanisms that generate and control oral-motor activities such as reflex-evoked and rhythmic jaw movements have been investigated with a variety of techniques. Extracellular unit recording, and intra-axonal, intracellular, and electromyographic recording in the behaving animal, in addition to anatomic techniques, have characterized the brain stem circuitry involved in pattern generation as well as provided a description of neuronal discharge during operation (Goldberg and Chandler 1990; Lund 1991; Nakamura and Katakura 1995). These studies have provided important insights into the brain stem control of oral-motor behaviors.

More recently, *in vitro* preparations have been used to investigate the factors that control discharge properties of motoneurons and interneurons that make up the brain stem circuits responsible for oral-motor pattern generation (Apenteng et al. 1995; Chandler et al. 1994; Katakura et al. 1995; Kogo et al. 1996). This biophysical level of investigation is necessary to understand the control of spatiotemporal discharge patterns of brain stem neurons during jaw movements.

Mesencephalic trigeminal sensory (Mes 5) neurons are critical components of the brain stem circuitry responsible for oral-motor behaviors. In the periphery these cells innervate jaw-closer muscle spindles and periodontal mechanoreceptors (Corbin and Harrison 1940; Jerge 1963), and centrally project to motoneurons and premotoneurons that control jaw musculature (Dessem and Taylor 1989; Luo et al. 1995). Therefore the electrical responses of Mes 5 neurons, which are controlled by intrinsic membrane properties, will influence both reflex-evoked and rhythmic jaw movements.

4-Aminopyridine (4-AP) and tetraethylammonium (TEA)-sensitive  $K^+$  currents are critical determinants of peripheral spike genesis (Kirchhoff et al. 1992) and axonal electrical properties in mammalian sensory cells (Bostock et al. 1981; Bowe et al. 1987; Kocsis et al. 1986, 1987). 4-AP, in particular, at axonal or peripheral sites causes repetitive discharge. In sensory neurons making up visceral ganglia (Stansfeld et al. 1986) and trigeminal root ganglia (Puil et al. 1989; Spigelman and Puil 1989), 4-AP application has likewise been shown to cause repetitive firing in previously rapidly accommodating cell bodies. These data on the effects of 4-AP suggest some degree of ion channel homogeneity at peripheral, axonal, and somatic locations in mammalian sensory neurons.

In the present work we have identified two distinct 4-AP-sensitive outward currents, one transient ( $I_{\text{TOC-S}}$ ) and one sustained ( $I_{4\text{-AP}}$ ), whose removal eliminates accommodation and results in repetitive firing in Mes 5 sensory neurons. In this effort TEA-sensitive currents have also been characterized, including a delayed rectifier ( $I_{\text{K-DR}}$ ) and a  $\text{Ca}^{2+}$ -dependent  $K^+$  current ( $I_{\text{K-Ca}}$ ) as well as a 4-AP- and TEA-insensitive fast transient outward current ( $I_{\text{TOC-F}}$ ). To attain our primary goal, understanding the contributions of individual  $K^+$  currents during excitation, we augmented electrophysiological methods with mathematical modeling. Although limited in scope, the model facilitated examination of the dynamic interaction of outward currents during excitation.

That Mes 5 somata may possess an integrative role during oral-motor activities imputes additional significance to the results of the present investigation. Such a role for Mes 5

stems from its unique location in the CNS and synaptic innervation (Alley 1973; Liem et al. 1992; Luo and Dessem 1995; Roberts and Witkovsky 1975). Under some circumstances, then, Mes 5 neurons may operate like traditional “integrate and fire” neurons in addition to typical sensory neurons (which generally do not receive synaptic contacts at the soma and do not discharge repetitively).

## METHODS

Electrical recordings were performed at room temperature on neurons obtained from neonatal rat brain stem slices (age 1–7 days). In some animals ( $n = 15$ ) texas red (2%, Molecular Probes, Eugene, OR) was injected into the superficial masseter and temporalis muscles (24 h before) for anterograde labeling of Mes 5 cells. Animals were anesthetized by halothane inhalation, decapitated, and dissected in oxygenated ice-cold cutting solution (see below for composition). Coronal slices (200  $\mu\text{m}$ ) were cut from the brain stem with the use of a vibratome (DSK microslicer, Ted Pella, Redding, CA) and placed into room-temperature incubation solution (see below). Slices were incubated at 37°C for 40 min.

## Solutions

Cutting solution was composed of (in mM) 126 NaCl, 3 KCl, 1.25  $\text{NaH}_2\text{PO}_4$ , 26  $\text{NaHCO}_3$ , 10 glucose, 1  $\text{CaCl}_2$ , 5  $\text{MgCl}_2$ , and 4 lactic acid (Schurr et al. 1988). Basic artificial cerebrospinal fluid recording solution contained (in mM) 124 NaCl, 3 KCl, 1.25  $\text{NaH}_2\text{PO}_4$ , 26  $\text{NaHCO}_3$ , 10 glucose, 2  $\text{CaCl}_2$ , and 2  $\text{MgCl}_2$ . Ionic substitutions were obtained by equimolar replacement of NaCl or other ionic species as indicated in the text. Compounds in concentrations  $\leq 3$  mM were added directly to recording solutions. Incubation solution was identical to recording solution but had additional 4 mM lactic acid (Schurr et al. 1988). All solutions were bubbled with 95%  $\text{O}_2$ -5%  $\text{CO}_2$  during the course of the experiment and maintained at  $\text{pH} \cong 7.3$  (22–24°C). Patch electrode solution contained (in mM) 9.0 NaCl, 140.0 KCl, 1.0  $\text{MgCl}_2$ , 10.0 *N*-2-hydroxyethylpiperazine-*N'*-2-ethanesulfonic acid buffer, 0.2 ethylene glycol-bis( $\beta$ -aminoethyl ether)-*N,N,N',N'*-tetraacetic acid, 5.0  $\text{K}_2$ -ATP, and 1.0  $\text{Na}_3$ -GTP,  $\text{pH} \cong 7.25$ , osmolarity adjusted to 280–290 mosmol. Lucifer yellow (0.1%, Sigma Chemical, St. Louis, MO) was added to small volumes of electrode internal solution and used to backfill electrode tips for fluorescence viewing.

## Identification of Mes 5 neurons

Mes 5 was identified under Nomarski optics as a collection of elliptical perikarya located dorsally in brain stem slices  $\sim 500$   $\mu\text{m}$  lateral to the midline. In early experiments, anterograde labeling of Mes 5 neurons by texas red was utilized to confirm that the area was indeed Mes 5 ( $n = 15$ ). In the rostrocaudal orientation, Mes 5 was first seen in slices containing the trigeminal motor nucleus and within 600  $\mu\text{m}$  rostral to this point. Mes 5 was easily distinguished from locus coeruleus and parabrachial neurons by morphology. Additionally, slow anomalous rectification during hyperpolarizing voltage commands was sufficient to ensure that a locus coeruleus neuron had not been mistakenly obtained (Henderson et al. 1982).

## Electrophysiological techniques

Slices were perfused with oxygenated recording solution (4 ml/min) while secured in a recording well mounted on a Zeiss fixed stage Axioskop equipped with bright-field, fluorescence, and Nomarski optics (Edwards et al. 1989). Additional visual resolution

was obtained by infrared video microscopy (Stuart et al. 1993). Patch electrodes fabricated from borosilicate glass capillary tubing (1.5 mm OD, 0.86 mm ID) had bath resistance of 3–7  $\text{M}\Omega$ . Voltage- and current-clamp experiments were performed with the use of an Axopatch-1D patch-clamp amplifier (Axon Instruments, Foster City, CA) in concert with pCLAMP acquisition software (version 6.0.3, Axon Instruments) running on a Pentium-class PC. Gigaseals ( $>1$   $\text{G}\Omega$ ) were formed and whole cell recording configuration obtained by suction and a short voltage pulse (buzz). All signals were grounded by a 3 M KCl-agar bridge electrode (Ag/AgCl wire) mounted in the recording well. A liquid junction potential of 1 mV was not corrected. On-line leak subtraction was not employed.

Whole cell capacitance ( $C_M$ ) was determined from the integral of high-resolution capacity current. Input resistance ( $R_N$ ) was estimated by the reciprocal slope of the steady-state current-voltage relation in its linear region around resting potential ( $\pm 10$  mV) obtained in voltage clamp, or from the steady-state voltage-current relation (in current clamp).  $R_N$  was utilized for off-line leak subtraction as indicated in the text.

Series resistance ( $R_S$ ) was calculated off-line from the time constant of the decay of the capacity transient ( $\tau \cong R_S C_M$ ). This calculation requires that the  $R_N$  of the cell be significantly greater than  $R_S$  [satisfied by  $R_N \geq (10 R_S)$  for cells included in voltage-clamp analysis].  $R_S$  was compensated up to 80% through the amplifier.

Mes 5 neurons are in general pseudounipolar, so space-clamp errors were expected to be minimal despite axonal and (in some cells) small, thin dendritic processes. The assertion of isopotentiality in Mes 5 neurons was verified by the adequacy of single-exponential fits to the decay of the capacity transient used to determine  $C_M$ . The time constant for the decay of the capacity transient was 0.228 ms in a typical cell with  $C_M = 20.0$  pF ( $R_S = 11.4$   $\text{M}\Omega$ , uncompensated).

## Modeling techniques

The Mes 5 model neuron was constructed as an isopotential excitable membrane coupled to a fluid compartment system according to the methods outlined in detail by Yamada et al. (1989). Our model represents a cell 26  $\mu\text{m}$  diam with  $C_M = 21$  pF whose plasmalemma expresses  $\text{Na}^+$  current ( $I_{\text{Na}}$ ), two  $\text{Ca}^{2+}$  currents ( $I_{\text{CaN}}$ ,  $I_{\text{CaT}}$ ), mixed cationic current ( $I_h$ ), four  $\text{K}^+$  currents ( $I_{4\text{-AP}}$ ,  $I_{\text{K-DR}}$ ,  $I_{\text{TOC-F}}$ , and  $I_{\text{TOC-S}}$ ), a  $\text{Ca}^{2+}$ -dependent  $\text{K}^+$  current ( $I_{\text{K-Ca}}$ ), and leakage current ( $I_{\text{LEAK}}$ ). Voltage-dependent currents were numerically reconstructed from voltage-clamp data according to modified Hodgkin and Huxley (1952) functions (HH model, see APPENDIX). Equations governing membrane potential ( $V_M$ ) trajectory and  $\text{Ca}^{2+}$  concentration dynamics are detailed in the APPENDIX. Simulations were performed on a Pentium-class PC with the use of a fourth-order Runge-Kutta numerical integrator (time step = 0.05 ms) (Stella II, HPS, Hanover, NH).

## RESULTS

Electrophysiological recordings were performed on 219 Mes 5 neurons (20 min to 1 h). The basic parameters measured in this database include resting potential of  $-56.0 \pm 0.5$  (SE) mV (minimum  $-45$  mV,  $n = 125$ );  $R_N = 344.6 \pm 18.3$   $\text{M}\Omega$  ( $\sim 75$   $\text{M}\Omega$  to 1  $\text{G}\Omega$ ,  $n = 138$ ); and membrane capacitance of  $22.0 \pm 1.9$  pF ( $\sim 10$ –48 pF,  $n = 124$ ).

## Current-clamp properties

At  $V_M$ s more negative than approximately  $-55$  mV, Mes 5 neurons displayed rapid accommodation in response to

depolarizing current (Fig. 1A, *left*). The spike emerged, at threshold, from a subthreshold damped oscillation of the  $V_M$  (Fig. 1A, *left, middle traces*). Increased current stimuli did not evoke spike trains in Mes 5 neurons from these negative holding potentials ( $-64$  mV, Fig. 1A, *left, top trace*). These responses resembled sensory neurons of the trigeminal root ganglia (Puil and Spigelman 1988; Puil et al. 1989).

The response of Mes 5 neurons to depolarizing currents was altered when the  $V_M$  was held at more positive levels (greater than  $-55$  mV) (Fig. 1A, *right*). As current stimuli were increased from the depolarized holding potential ( $-49$  mV), the cell in Fig. 1 subsequently responded with a transient spike burst consisting of five action potentials (Fig. 1A, *right, top trace*). The data suggested that sustained depolarization to  $-49$  mV removed an outward current (pre-

sumably by inactivation). This putative inactivating current was normally available from hyperpolarized  $V_M$ s and was effective in suppressing the emergence of spike bursts (for 100–200 ms after the onset of the stimulus) from these holding levels.

Inactivating outward currents in sensory neurons are of two basic types: those sensitive to TEA (generally resembling the ubiquitous delayed rectifier with some degree of slow inactivation) or transient outward (A-type) currents (generally sensitive to 4-AP in mM concentrations). To investigate whether putative transient outward currents (TOCs) prevented spike bursts in Mes 5 from hyperpolarized potentials (less than  $-55$  mV), 4-AP was applied and the experiments of Fig. 1A were repeated to see whether spike bursts could be subsequently evoked from these holding levels.

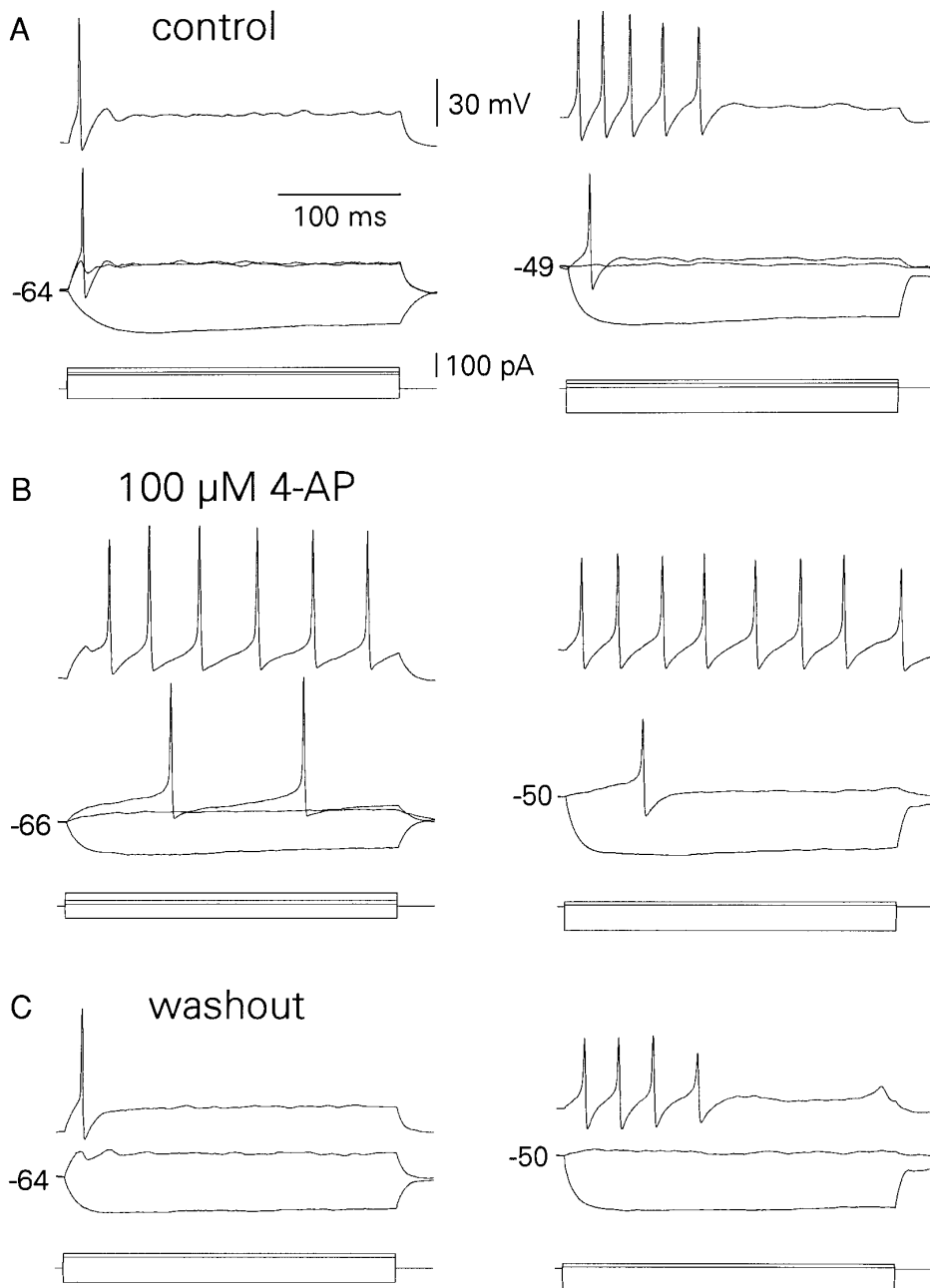


FIG. 1. Effects of holding potential and 4-aminopyridine (4-AP) application on membrane responses to depolarizing current injection. All records from the same cell. *A*: effect of holding potential. In response to subthreshold depolarizing currents from  $-64$  mV (*left*), the cell exhibited damped oscillations. As current was increased to threshold and beyond, a single spike emerged (*middle* and *top*). At  $-49$  mV (*right*), rheobasic current evoked a single spike (*middle*). Suprathreshold current injection caused a transient spike burst that lasted  $\sim 120$  ms (*top*). *B*: effect of 100  $\mu$ M 4-AP. At  $-66$  mV (*left*), action potentials were evoked at threshold (*middle*). Suprathreshold currents evoked repetitive firing preceded by a notchlike repolarization (*top*). At  $-50$  mV (*right*), the cell was spontaneously active (*middle*). Suprathreshold currents evoked sustained repetitive spiking without the "notch" (*top*). *C*: washout.

4-AP application (50  $\mu\text{M}$  to 2 mM,  $n = 27$ ) mediated multiple effects on Mes 5 neurons, as illustrated by the cell in Fig. 1B. At  $-66$  mV, rheobase was reduced and the action potential at threshold was not normally followed by a damped oscillation but rather by subsequent spikes (Fig. 1B, *left, top and middle traces*). Increased stimulus current evoked sustained repetitive firing from either  $V_M$  (Fig. 1B, *top traces*). Sustained spike discharge in 4-AP could be maintained for  $>100$  s with minimal bias current ( $n = 3$ , not shown). The data suggested that 4-AP application 1) blocked the outward current whose putative inactivation at  $-49$  mV allowed the emergence of spike bursts and 2) blocked some other outward current that may have been responsible for ultimately causing accommodation at depolarized potentials.

An additional feature of excitation from  $-66$  mV was the presence of a transient repolarizing "notch" preceding the spike train in the presence of 4-AP (Fig. 1B, *left, top trace*). This notchlike feature is commonly associated with activation of a fast TOC (Hsiao and Chandler 1995; Jahnsen and Llinas 1984; Segal et al. 1984) and therefore suggests the presence of a 4-AP-insensitive fast TOC. This notch was never observed in control. At depolarized holding levels ( $-50$  mV) no transient repolarizing notch preceded the spike train, suggesting that the putative 4-AP-insensitive fast TOC inactivated. The effects of 4-AP were reversible (Fig. 1C).

To investigate the role of TEA-sensitive outward currents in the control of spiking behavior, cells were depolarized by current injection in control and TEA conditions (10–30 mM). The amplitude and duration of the action potential were increased and the afterhyperpolarization was reduced in TEA (Fig. 2, A and B).

TEA did not elicit repetitive firing in the majority of Mes 5 neurons tested (16 of 19) (Fig. 2B). However, TEA application in 7 of 19 cells caused plateau-like action potentials to emerge as the current stimulus was increased (Fig. 2B, *top trace*). The plateau potentials were sensitive to block by 50  $\mu\text{M}$   $\text{Cd}^{2+}$ , indicating their dependence on  $\text{Ca}^{2+}$  activation (not shown). TEA's effects were reversible (Fig. 2C).

Action potentials of Mes 5 neurons were blocked by tetro-

dotoxin (TTX) application (not shown) and fast inward currents in voltage-clamp conditions were always sensitive to TTX, in contrast to sensory neurons of other cerebrosplinal ganglia (Kostyuk et al. 1981b; Puil and Spigelman 1988) that often express TTX-insensitive fast  $\text{Na}^+$  current.

The induction of sustained repetitive firing has been associated with pharmacological attenuation of the M current (Adams et al. 1982). To test for this possibility in Mes 5, muscarine was applied (5–20  $\mu\text{M}$ ) in five cells, but the drug did not exhibit any discernible effect (not shown).

#### Voltage-clamp analysis of the effects TEA and 4-AP on sustained outward currents

Whole cell voltage clamp was employed to examine the effects of the pharmacological agents 4-AP and TEA on the intrinsic currents of Mes 5 neurons.  $V_M$  was held at  $-40$  mV (to inactivate TOCs) in 0.5  $\mu\text{M}$  TTX and 50  $\mu\text{M}$   $\text{Cd}^{2+}$  and stepped to levels between  $-70$  and  $-10$  mV for  $\sim 1$  s to measure the steady-state current in control and either TEA or 4-AP conditions. Application of TEA (20 mM) caused a large decrease in the outwardly rectifying currents evoked at  $V_M$ s greater than  $-46$  mV (Fig. 3, A and B, *left*).

4-AP (100  $\mu\text{M}$ ) was used to identify 4-AP-sensitive sustained current during voltage-clamp experiments on the basis of our observation that 50  $\mu\text{M}$  4-AP was the minimum dose required to produce sustained repetitive firing in current-clamp conditions 50% of the time. In contrast to TEA, 4-AP reduced outward currents evoked by voltage steps to potentials closer to the holding level ( $-54$  to  $-30$  mV), which recovered in washout (Fig. 3C). The reduction of currents in this range by 100  $\mu\text{M}$  4-AP is reflected in the extended linear region of the steady-state current-voltage plot (Fig. 3B, *right*). 4-AP caused a slight reduction in the sustained outward currents at very depolarized potentials (greater than  $-25$  mV) that did not recover in this cell (Fig. 3C).

To quantify the effects of 4-AP and TEA on the rectifying properties of Mes 5 neurons, we compared each agent's ability to reduce the active currents evoked at  $-50$  and  $-10$

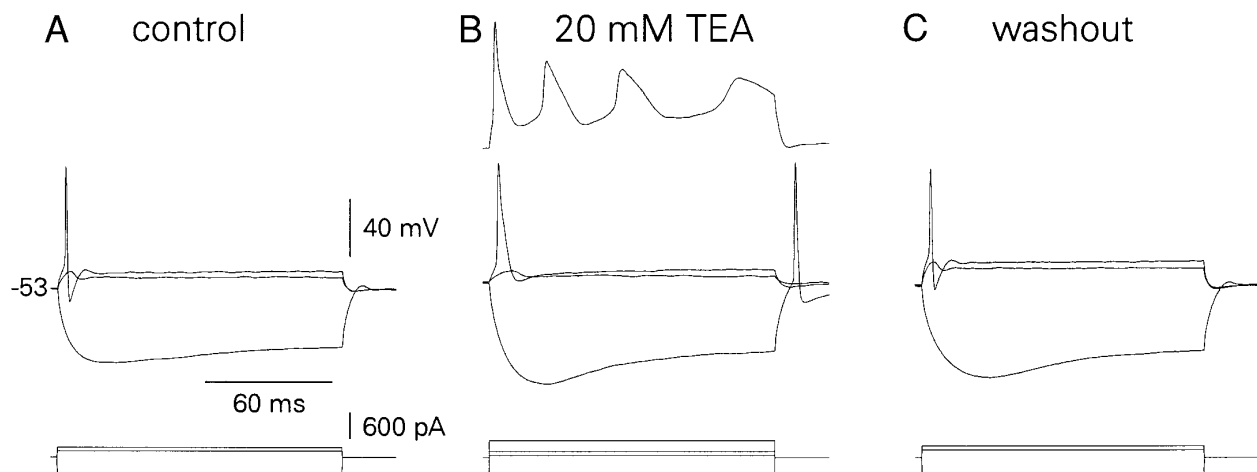


FIG. 2. Effect of tetraethylammonium (TEA) on membrane responses. A: membrane responses in control. B: in 20 mM TEA, amplitude and duration of the spike increased and afterhyperpolarization decreased (*middle*). Suprathreshold currents evoked  $\text{Ca}^{2+}$ -mediated action potentials and plateau potentials (*top*). C: washout.

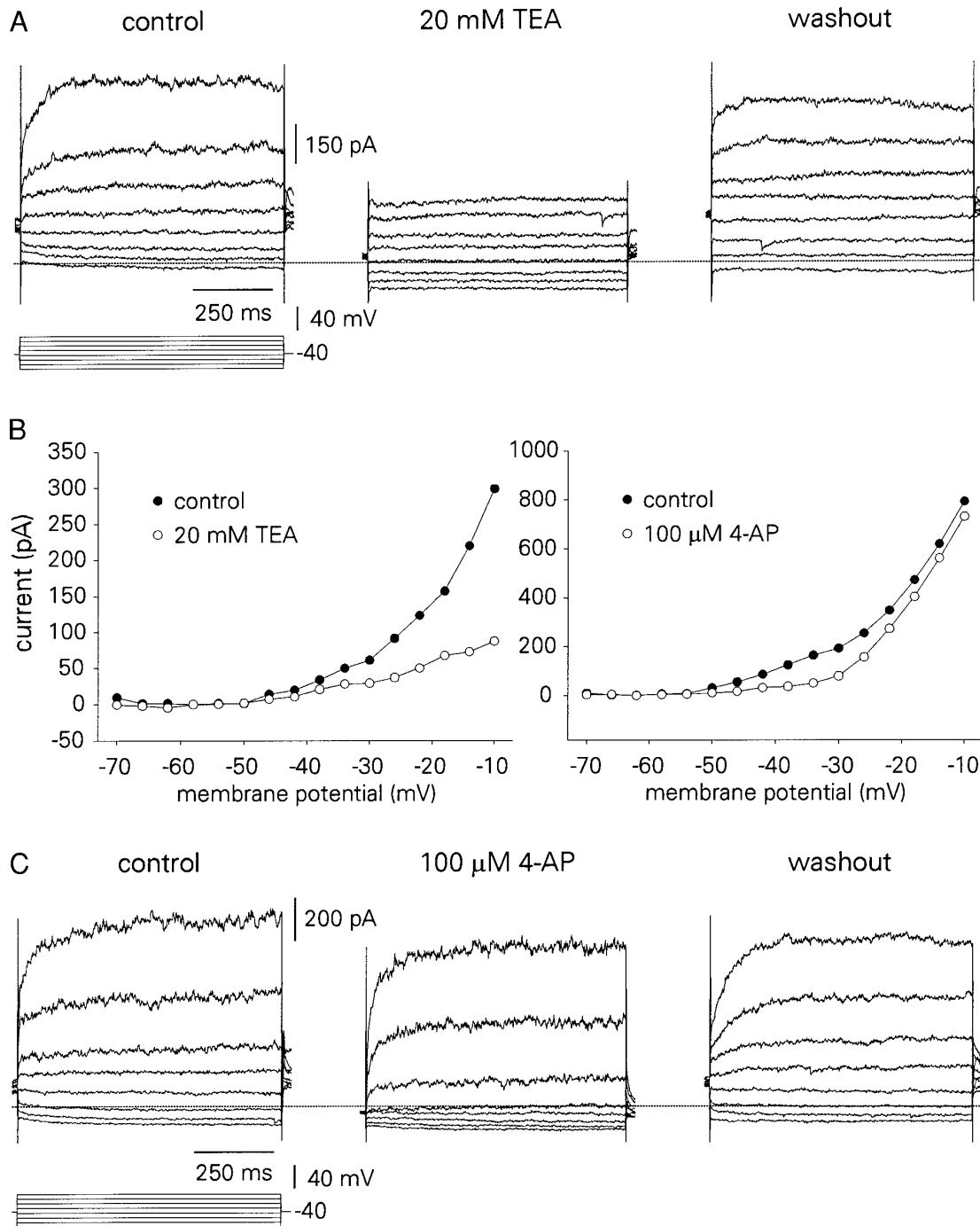


FIG. 3. Voltage-clamp effects TEA and 4-AP. *A* and *C*: in  $0.5 \mu\text{M}$  tetrodotoxin (TTX) and  $50 \mu\text{M}$   $\text{Cd}^{2+}$ . Dotted line: 0 current. *A*: from  $-40 \text{ mV}$ ,  $20 \text{ mM}$  TEA reversibly reduced outward currents evoked by command potentials to uppermost levels (waveform below). *B*: leak subtracted steady-state current-voltage curves showing control ( $\bullet$ ) vs. TEA (*left*,  $\circ$ ) and 4-AP (*right*,  $\circ$ ) from *A* and *C*, respectively. *C*: from  $-40 \text{ mV}$ ,  $100 \mu\text{M}$  4-AP reduced outward currents evoked by command potentials near to rest (waveform below), which was reversible in this voltage range.

mV. At  $-50 \text{ mV}$ ,  $20 \text{ mM}$  TEA reduced active current by  $59.8 \pm 4.5\%$  (mean  $\pm$  SE,  $n = 11$ ), whereas  $100 \mu\text{M}$  4-AP caused an  $82.2 \pm 3.6\%$  reduction ( $n = 17$ ). This difference was statistically significant ( $P < 0.001$ ). At  $-10 \text{ mV}$ , TEA caused a  $70.0 \pm 3.0\%$  reduction ( $n = 11$ ) in active current, in contrast to 4-AP, which reduced the current by  $33.1 \pm 3.1\%$  ( $n = 17$ ). This difference was also statistically significant ( $P < 0.001$ ). These data indicated the presence

of two sustained outward currents that were distinguished by pharmacology and voltage dependence.

#### 4-AP-sensitive sustained current

The following protocol was employed to isolate the 4-AP-sensitive sustained current ( $I_{4\text{-AP}}$ ) and measure its voltage-dependent activation properties. The cell, in  $0.5 \mu\text{M}$  TTX

and  $50 \mu\text{M Cd}^{2+}$ , was stepped for 800-ms intervals to potentials in the range of  $-70$  to  $-26$  mV from the holding potential of  $-40$  mV (Fig. 4A, *left*). This set of commands was repeated in  $100 \mu\text{M}$  4-AP (Fig. 4A, *middle*) and the current records were digitally subtracted from control to yield  $I_{4\text{-AP}}$  (Fig. 4A, *right*). Data were corrected for leakage currents. The activation curve was obtained from normalized conductance of  $I_{4\text{-AP}}$  plotted versus  $V_M$  (Fig. 4B, *left*). The composite activation curve is shown in Fig. 4B, *right* [voltage of half-maximal activation ( $V_{1/2\text{-MAX}}$ ) =  $-48.0$  mV,  $k = -3.9$ ,  $n = 13$ ].  $I_{4\text{-AP}}$  activates at approximately  $-60$  mV and is fully activated by  $-30$  mV, which is consistent with 4-AP's reduction of active current between  $-54$  and  $-30$  mV in the steady-state current-voltage curve (Fig. 4B, *right*).

The kinetics of  $I_{4\text{-AP}}$  was determined by tail current analysis.  $V_M$  was held at  $-40$  mV (where  $I_{4\text{-AP}}$  is 89% activated and  $I_{K\text{-DR}}$  is not yet active) and stepped for 500-ms intervals to potentials from  $-70$  to  $-46$  mV to measure the time course of deactivation (Fig. 5A). Hyperpolarization-acti-

vated mixed cationic current ( $I_h$ ) is only 6% activated at  $-70$  mV ( $n = 6$ ), so would be expected to contribute minimally to the tail currents of  $I_{4\text{-AP}}$  at this level. We chose to measure deactivation of the current in a limited voltage range rather than utilize the subtracted 4-AP-sensitive currents over the entire range, because the latter method introduced an intolerable amount of noise for use in curve fitting algorithms. Leakage current was factored into the fitting algorithm as a linear function of driving force. Deactivation of  $I_{4\text{-AP}}$  from  $-40$  mV was biexponential in character and voltage dependent ( $n = 11$ ). The basic HH model was therefore modified to include the sum of two gating variables ( $n_1$  and  $n_2$ ) whose contributions are weighted by factor "a" (between 0 and 1)

$$I_{4\text{-AP}} = g_{4\text{-AP-MAX}}[an_1 + (1 - a)n_2](V_M - E_K)$$

Reconstructed  $I_{4\text{-AP}}$  is illustrated by the smooth traces overlying raw data (Fig. 5A). The decay of the current was more rapid as the membrane was depolarized (Fig. 5B). The slow

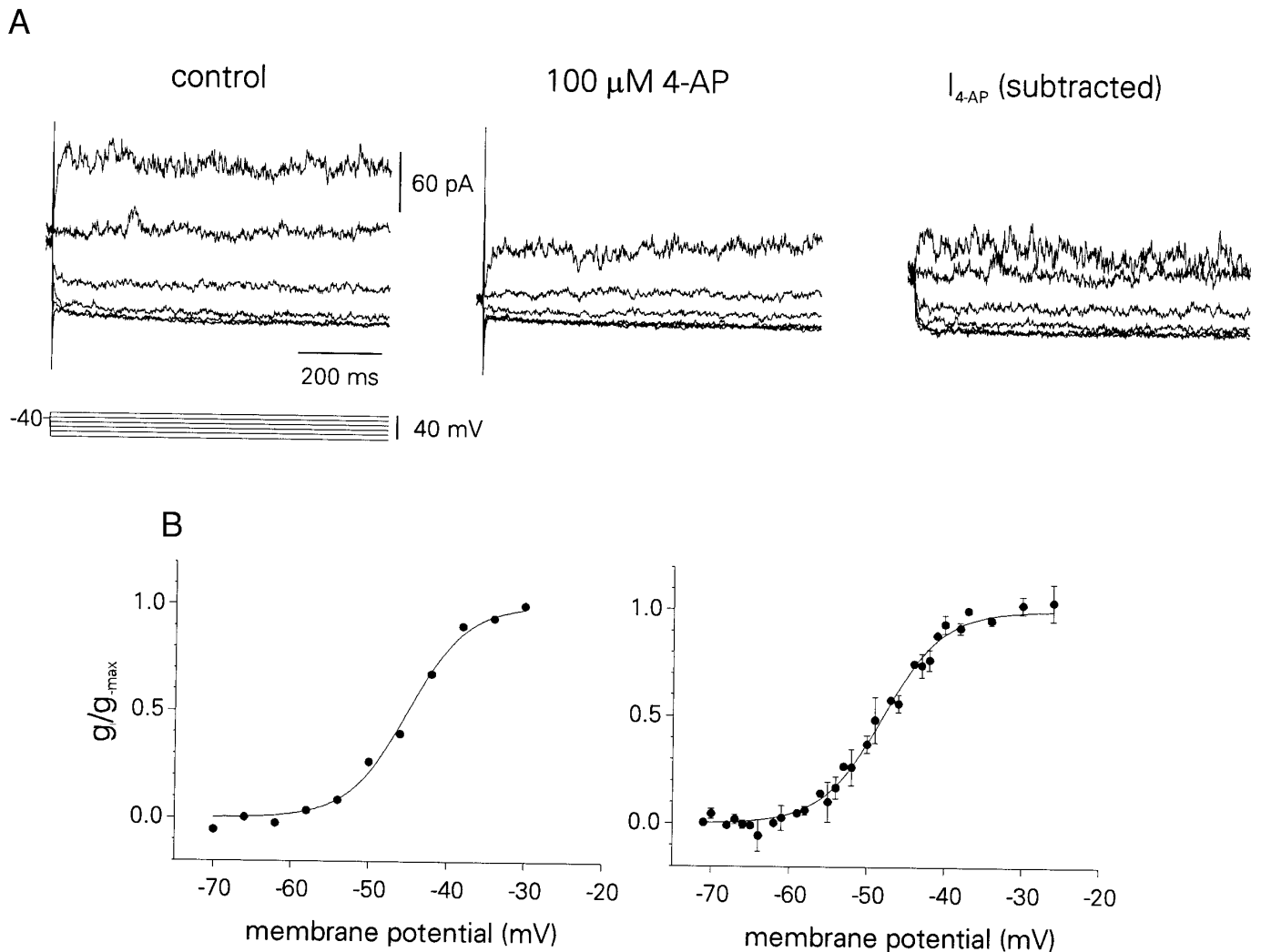


FIG. 4. Voltage-dependent properties of the sustained outward 4-AP-sensitive current  $I_{4\text{-AP}}$ . *A*: outward currents evoked by command potentials (*bottom*) delivered from  $-40$  mV in  $0.5 \mu\text{M}$  TTX and  $50 \mu\text{M}$   $\text{Cd}^{2+}$  in control (*left*) and  $100 \mu\text{M}$  4-AP (*middle*) conditions. Digital subtraction of 4-AP from control represents  $I_{4\text{-AP}}$  (*right*). *B*: normalized conductance ( $g/g_{\text{max}}$ ) plotted vs. command potential for the cell in *A* (*left*) and the aggregate curve (*right*): voltage of half-maximal activation ( $V_{1/2\text{-MAX}}$ ) =  $-48.0$  mV,  $k = -3.9$  ( $n = 13$ ).

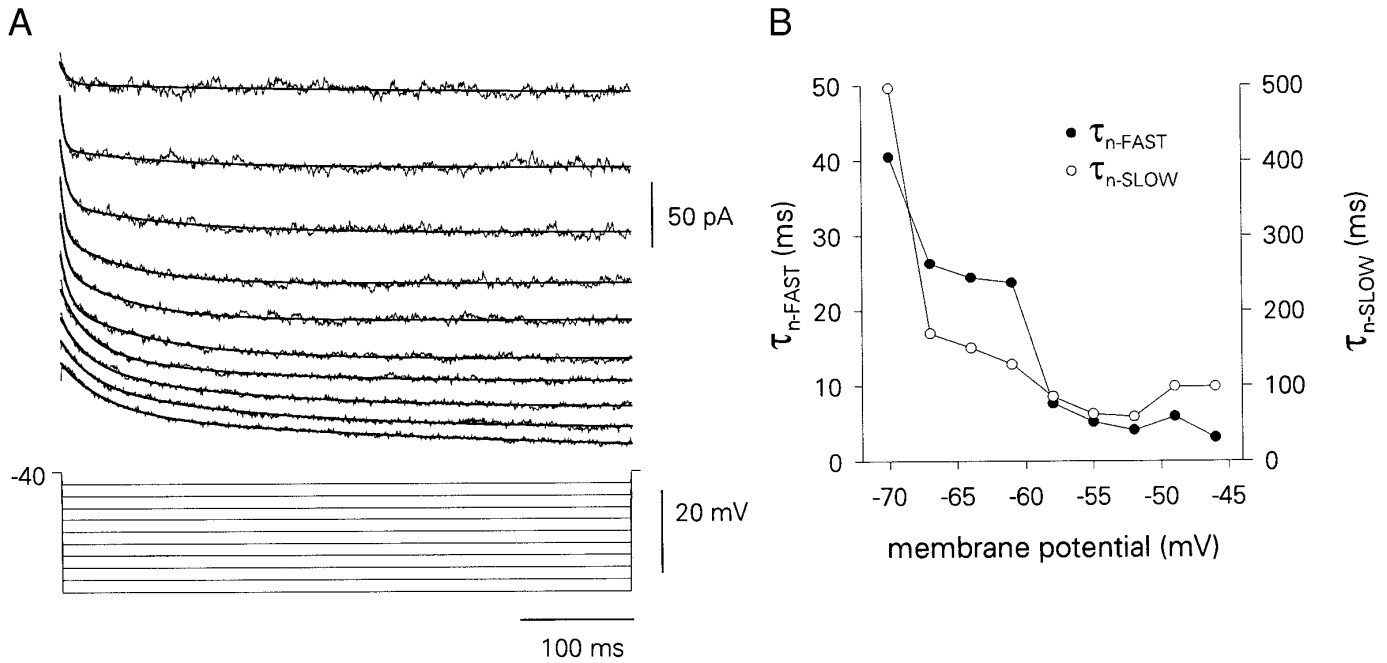


FIG. 5. Kinetic reconstruction of  $I_{4-AP}$ . *A*: current records in  $0.5 \mu\text{M}$  TTX and  $50 \mu\text{M}$   $\text{Cd}^{2+}$  (rough traces) evoked by the voltage protocol (*bottom*), and the reconstructed currents overlying the data (smooth traces). *B*: voltage-dependent time constants for fast ( $\tau_{n-FAST}$ , ●, left axis) and slow ( $\tau_{n-SLOW}$ , ○, right axis) components of  $I_{4-AP}$  plotted vs. command potential.

time constant ( $\tau_{n-SLOW}$ ) was  $\sim 100$ – $500$  ms, 1 order of magnitude larger than its fast counterpart ( $\tau_{n-FAST}$ , 3–40 ms) ( $n = 11$ ).

#### TEA-sensitive current

To isolate the TEA-sensitive sustained current and measure its activation properties, the following protocol was applied. In  $0.5 \mu\text{M}$  TTX and  $50 \mu\text{M}$   $\text{Cd}^{2+}$ , 100- to 200-ms command potentials in the range of  $-70$  to  $+44$  mV were delivered in control and TEA conditions from holding potentials of  $-40$  or  $-30$  mV (Fig. 6*A*). The more positive potential was occasionally required to minimize the contribution of the fast TOC, which, although largely inactivated at  $-40$  mV, was evoked to a small extent at very depolarized levels. Traces were corrected for leakage currents. The normalized conductance of the TEA-sensitive active current ( $I_{K-DR}$ ) obtained by subtraction (Fig. 6*A*, *right*) was plotted versus command potential (Fig. 6*B*, *left*). The composite activation curve is shown in Fig. 6*B*, *right* ( $V_{1/2-MAX} = -4.2$  mV,  $k = -12.9$ ,  $n = 4$ ).  $I_{K-DR}$  activated above  $-40$  mV and was fully activated by  $+40$  mV, consistent with TEA's block of outward rectification on the steady-state current-voltage curve positive to  $-42$  mV (Fig. 3*B*, *left*).

The kinetics of  $I_{K-DR}$  was characterized from outward currents evoked within 20–30 ms at command potentials greater than  $-19$  mV (Fig. 7*A*). This short time frame generated better kinetic fits to the onset time course of  $I_{K-DR}$  and produced more realistic action potentials in the model.  $I_{4-AP}$  is fully activated in the voltage range used to fit  $I_{K-DR}$  and is therefore factored into the reconstructions, with leakage current, as a linear function of driving force. The exponent of the activation gating variable ( $p$ ) in the

HH model was varied between 1 and 4 and the best fit was obtained for a first-order process. The final expression

$$I_{K-DR} = g_{K-DR-MAX} p (V_M - E_K)$$

described  $I_{K-DR}$  (Fig. 7*A*). Activation of the current was more rapid as the  $V_M$  was depolarized (Fig. 7*B*) ( $n = 5$ ).

#### TOCs

TOCs were evoked by 3-s depolarizing command potentials in the range of  $-70$  to  $+50$  mV following 1-s prepulses to  $-100$  mV (Fig. 8*Aa*) in modified recording solution containing  $0.5 \mu\text{M}$  TTX,  $20$  mM TEA,  $3$  mM  $\text{Cs}^+$ , and  $100 \mu\text{M}$   $\text{Cd}^{2+}$  to block active currents ( $I_{Na}$ ,  $I_{K-DR}$ ,  $I_h$ , and  $\text{Ca}^{2+}$  and  $\text{Ca}^{2+}$ -dependent currents). Note that TOCs in Mes 5, in contrast to trigeminal root ganglion sensory neurons (Spigelman and Puil 1989), were not sensitive to TEA. Identical voltage commands were applied from the holding potential ( $-40$  mV) to evoke leakage current and  $I_{4-AP}$  (Fig. 8*Ab*). Subtracted current [Fig. 8*A(c)*] was defined as the TOC. The decay time course of the TOC evoked at  $V_M$ s above  $-10$  mV was characterized by rapid and slow phases. The rapid decay phase lasted 10–60 ms. The slow decay phase reached steady state after several seconds [Fig. 8*A(c)*].

The TOCs exhibited differential pharmacological sensitivity to 4-AP (Fig. 8*B*). 4-AP at concentrations  $\geq 500 \mu\text{M}$  completely blocked the slow component of the TOC [Fig. 8, *B(a)* and *B(b)*] ( $n = 16$ ). The resultant current in 4-AP ( $I_{TOC-F}$ ) decayed according to a single fast exponential function ( $\tau = 10.2$  ms) [Fig. 8*B(b)*]. The effects of 4-AP were partially reversible [Fig. 8*B(d)*]. A digital subtraction of  $I_{TOC-F}$  [(*b*)] from control [(*a*)] yielded the 4-AP-sensitive slow TOC ( $I_{TOC-S}$ ) [Fig. 8*B(c)*], which inactivated expo-

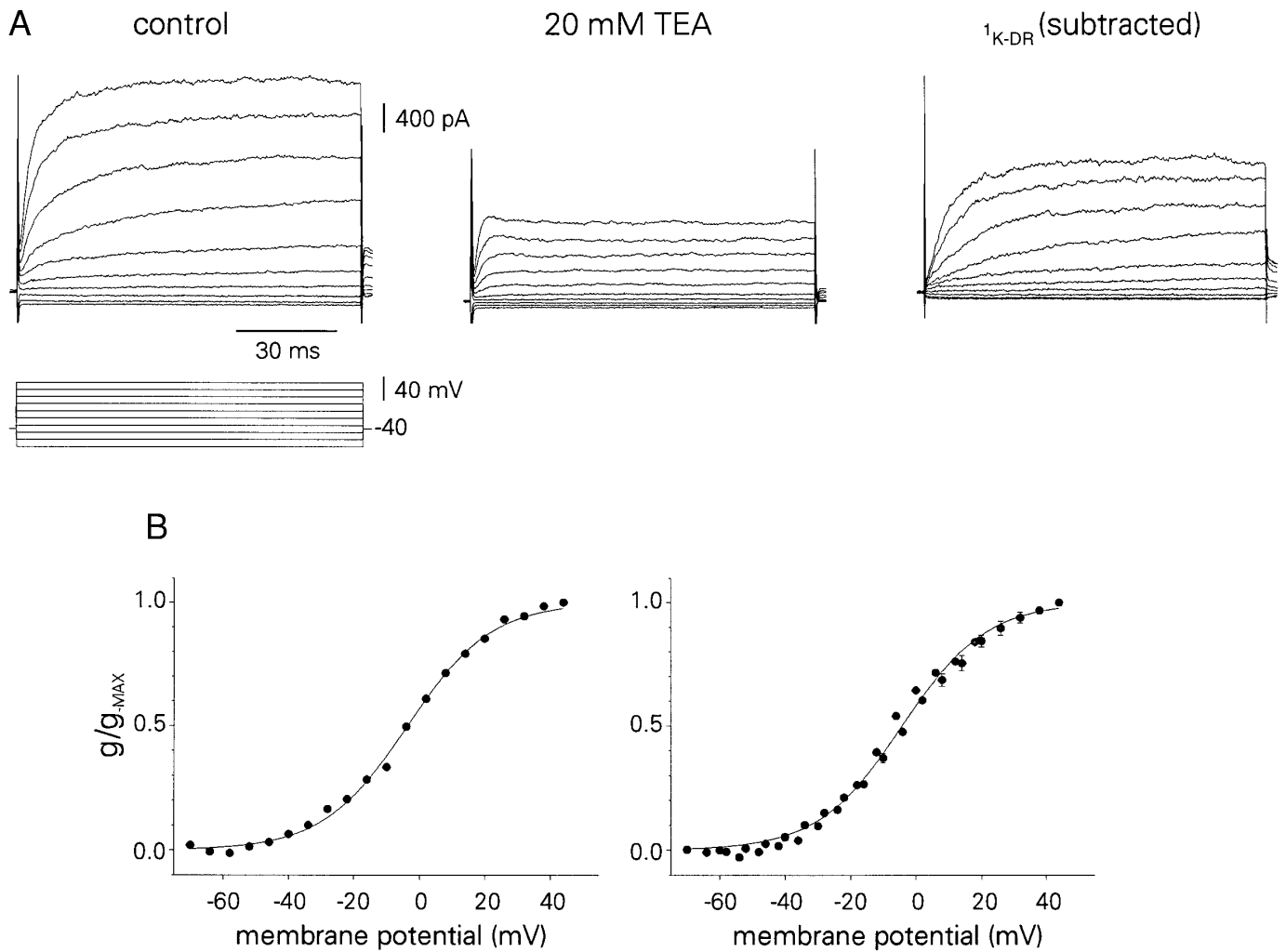


FIG. 6. Voltage dependence of TEA-sensitive delayed rectifier current ( $I_{K-DR}$ ). *A*: outward currents evoked by command potentials delivered from  $-40$  mV in  $0.5 \mu\text{M}$  TTX and  $50 \mu\text{M}$   $\text{Cd}^{2+}$  in control (*left*) and  $20$  mM TEA (*middle*) conditions. Digital subtraction of TEA from control represents  $I_{K-DR}$  (*right*). *B*: normalized conductance ( $g/g_{\text{MAX}}$ ) plotted vs. command potential for the cell in *A* (*left*) and the aggregate curve (*right*):  $V_{1/2-\text{MAX}} = -4.2$  mV,  $k = -12.9$  ( $n = 4$ ).

nentially ( $\tau = 124.0$  ms). The decay of  $I_{\text{TOC-S}}$  in this particular cell was relatively fast at  $+50$  mV.

The voltage dependence of  $I_{\text{TOC-F}}$  and  $I_{\text{TOC-S}}$  was determined in solutions containing 4-AP, which permitted separation of the currents (Fig. 9, *A-E*). The peak conductance of  $I_{\text{TOC-F}}$  recorded in 4-AP (Fig. 9*B*) was normalized and plotted versus command potential (Fig. 9*E*,  $\circ$ ).  $I_{\text{TOC-F}}$  activated positive to  $-40$  mV and approached its maximal activation above  $+40$  mV [Fig. 9*F*,  $\circ$ , shows composite data ( $n = 5$ ):  $V_{1/2-\text{MAX}} = 5.0$  mV,  $k = -15.4$ ]. Normalized peak conductance of  $I_{\text{TOC-S}}$  (obtained by subtraction, Fig. 9*C*) was also plotted versus command potential (Fig. 9*E*,  $\bullet$ ).  $I_{\text{TOC-S}}$  activated above  $-60$  mV and reached its plateau at approximately  $-20$  mV (Fig. 9*F*,  $\bullet$ :  $V_{1/2-\text{MAX}} = -34.7$  mV,  $k = -10.9$ ). Note that the fast time scale of Fig. 9*C* obscures the slow inactivation of  $I_{\text{TOC-S}}$ .

Voltage dependence of inactivation was measured as the normalized peak current at  $+10$  mV following 1-s voltage commands to levels between  $-110$  and  $-26$  mV. Inactivation of  $I_{\text{TOC-F}}$  (Fig. 9*E*,  $\square$ ) and  $I_{\text{TOC-S}}$  (Fig. 9*E*,  $\blacksquare$ ) was similar. Therefore the inactivation data displayed in Fig. 9*D*

were not separated. The parameters of the smooth inactivation curve in Fig. 9*F* (for composite TOCs) are:  $V_{1/2-\text{MAX}} = -62.0$  mV,  $k = 10.3$  ( $n = 5$ ).

Kinetic reconstruction of TOCs was accomplished by isolating the composite TOC as in Fig. 8*A*, then fitting with a standard HH model that included  $I_{\text{TOC-F}}$  and  $I_{\text{TOC-S}}$  (Fig. 10*A*).  $I_{\text{TOC-S}}$  was modeled as the product of first-order activation and inactivation gating variables and  $I_{\text{TOC-F}}$  as the product of a third-order activation gating variable and a first-order inactivation gating variable

$$I_{\text{TOC}} = I_{\text{TOC-S}} + I_{\text{TOC-F}}$$

$$I_{\text{TOC-S}} = g_{\text{TOC-S-MAX}} t_s g_s (V_M - E_K)$$

$$I_{\text{TOC-F}} = g_{\text{TOC-F-MAX}} (t_f)^3 g_f (V_M - E_K)$$

TOCs activated more rapidly as the membrane was depolarized (Fig. 10*B*,  $n = 4$ ). Accurate fits to the data were obtained with the use of a voltage-independent slow time constant ( $\sim 0.5$  s) for inactivation of  $I_{\text{TOC-S}}$  although in some cells this time constant showed some voltage dependence, e.g., Fig. 8*B(c)* and a voltage-dependent fast time constant for inactivation of  $I_{\text{TOC-F}}$  (Fig. 10*B*,  $n = 4$ ).

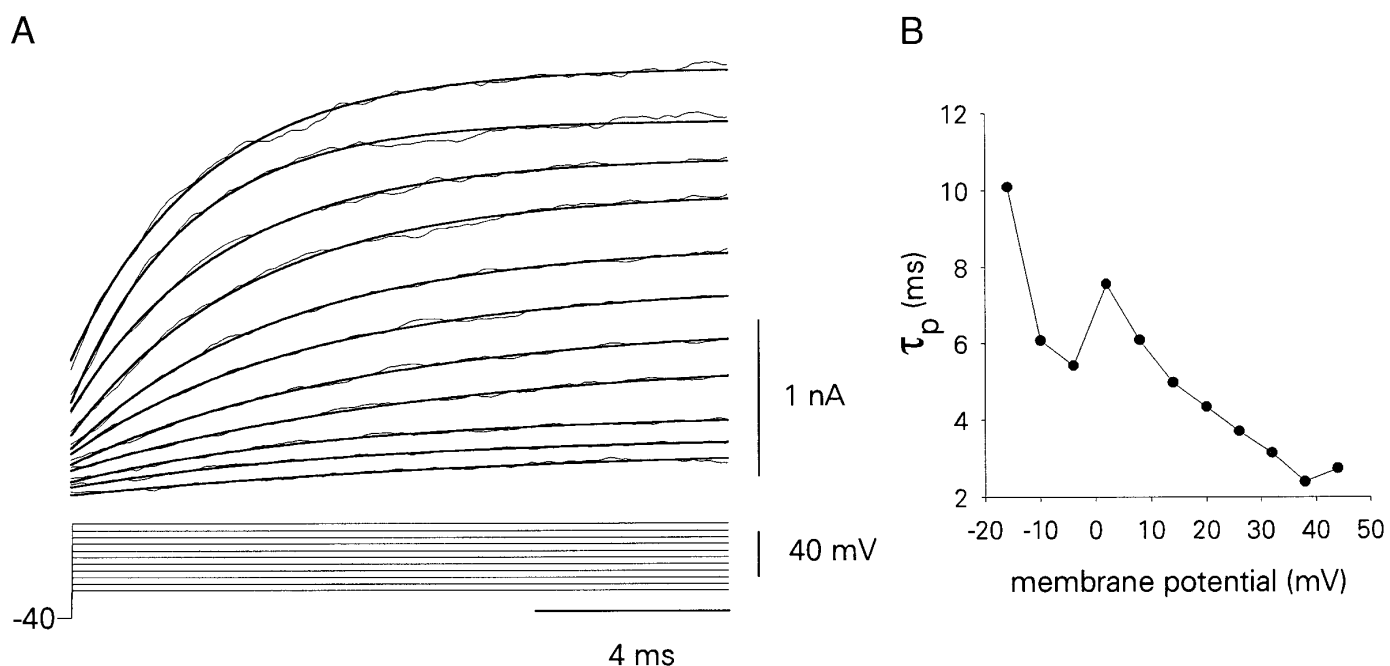


FIG. 7. Kinetic reconstruction of  $I_{K-DR}$ . *A*: current records in  $0.5 \mu\text{M}$  TTX and  $50 \mu\text{M}$   $\text{Cd}^{2+}$  (rough traces) evoked by the voltage protocol (*bottom*). Reconstructed currents are shown overlaying the data (smooth traces). *B*: voltage-dependent time constant  $\tau_p$  plotted vs. command potential.

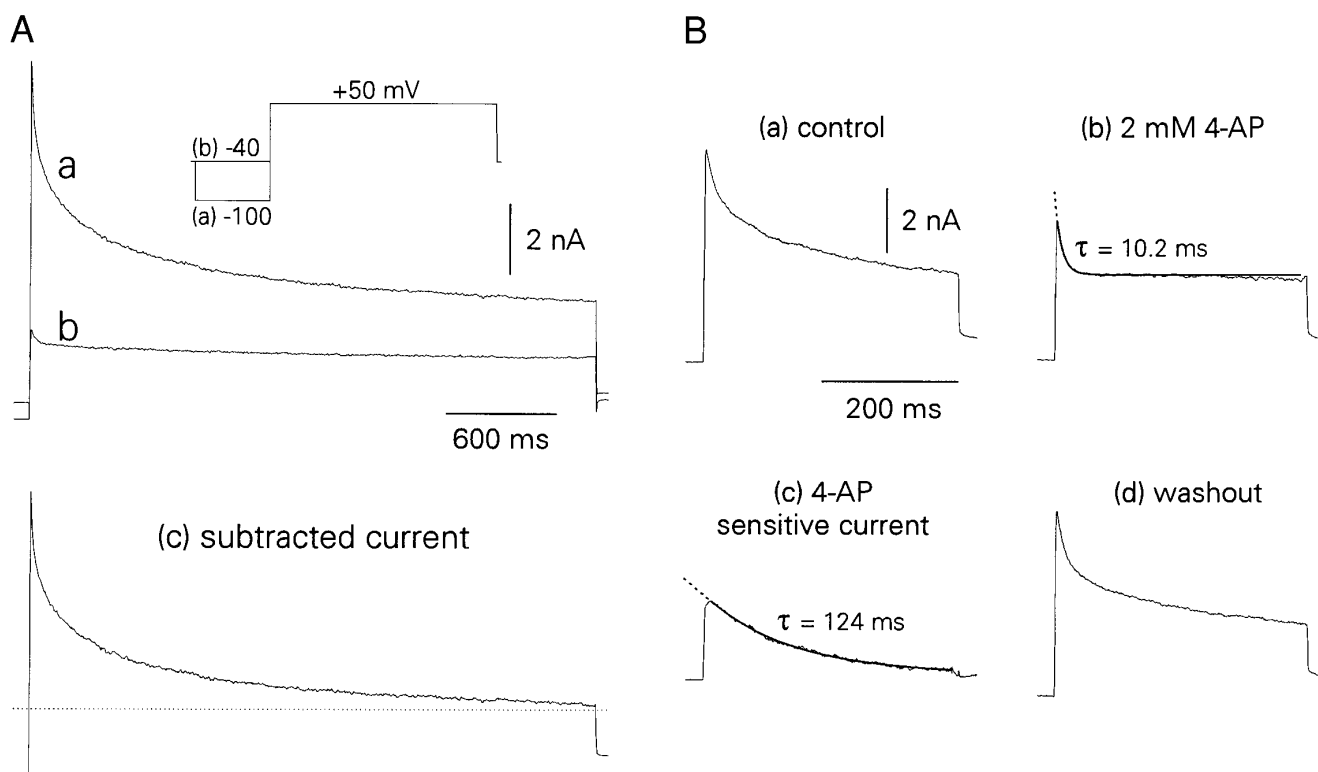


FIG. 8. Isolation of transient outward currents (TOCs). *A* and *B*: in  $0.5 \mu\text{M}$  TTX,  $100 \mu\text{M}$   $\text{Cd}^{2+}$ ,  $20 \text{ mM}$  TEA, and  $3 \text{ mM}$   $\text{Cs}^+$ . *A*: current response at  $+50 \text{ mV}$ , stepped from the holding potential of  $-40 \text{ mV}$  [(*b*)] was subtracted from the current response at  $+50 \text{ mV}$  following a 1-s hyperpolarizing step to  $-100 \text{ mV}$  [(*a*)] to obtain the TOC [(*c*)]. TOC inactivated with rapid and slow phases, which is highlighted by the slow time scale of *A*. *B*: biexponentially decaying TOC (isolated as in *A*) in control [(*a*)] was reduced to a single rapidly decaying TOC in  $2 \text{ mM}$  4-AP ( $I_{\text{TOC-F}}$ ,  $\tau = 10.2 \text{ ms}$ , exponential fit of the decay is superimposed on the data,  $\cdots$  is an extrapolation). The effects of 4-AP on the TOC were partially reversible [(*d*)]. The 4-AP-sensitive component of the TOC was obtained by subtraction [(*c*)],  $I_{\text{TOC-S}}$ ,  $\tau = 124 \text{ ms}$ , exponential fit of the decay is superimposed].

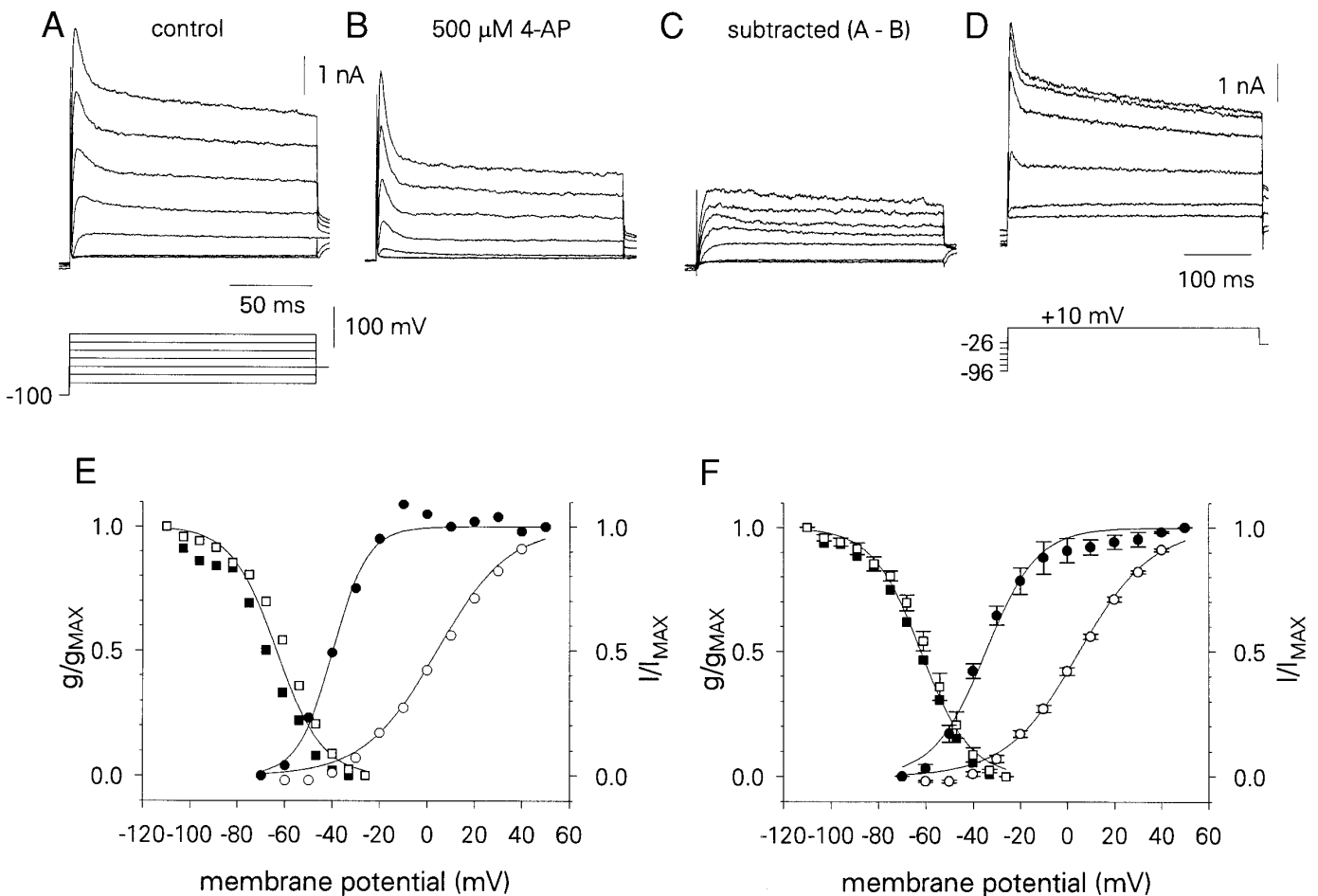


FIG. 9. Voltage-dependent properties of  $I_{TOC-F}$  and  $I_{TOC-S}$ . A–C: isolation of  $I_{TOC-F}$  and  $I_{TOC-S}$  as in Fig. 8. D: TOCs evoked at +10 mV following variable level 1-s prepulses as indicated (waveform at bottom) to assess inactivation properties. E and F: activation of  $I_{TOC-F}$  (○) and  $I_{TOC-S}$  (●) for the cell in A–D (E) or aggregate data (F). Activation parameters for  $I_{TOC-F}$  are:  $V_{1/2-MAX} = 5.0$  mV,  $k = -15.4$  ( $n = 5$ ); for  $I_{TOC-S}$  they are:  $V_{1/2-MAX} = -34.7$  mV,  $k = -10.9$  ( $n = 5$ ). Inactivation properties as assessed by normalized current ( $I/I_{MAX}$ , right axis) did not differ markedly between  $I_{TOC-F}$  and  $I_{TOC-S}$ :  $V_{1/2-MAX} = -62.0$  mV,  $k = 10.3$  ( $n = 5$ ).

### $Ca^{2+}$ -dependent outward current

$Ca^{2+}$ -dependent outward current ( $I_{K-Ca}$ ) was isolated by blocking  $Ca^{2+}$  influx with 50–100 μM  $Cd^{2+}$  ( $n = 6$ ) or by perfusion in low- $Ca^{2+}$  solution (0.5 mM) with equimolar  $Mg^{2+}$  substitution ( $n = 8$ ) (Fig. 11A).  $I_{K-Ca}$  was then obtained by subtraction (Fig. 11B, left) and on average constituted ~20% of the total outward current evoked positive to –30 mV (Fig. 11B, right,  $n = 14$ ).  $I_{K-Ca}$  was TEA sensitive (not shown). A standard HH expression was employed to model  $I_{K-Ca}$  (APPENDIX) because it was adequate to fit the data (not shown).

### Modeling results

The top traces in Fig. 12, A–C, represent  $V_M$  responses of the model cell to –110- and +100- pA current injection in control, reduced  $I_{TOC-S}$ , or reduced  $I_{4-AP}$  conditions, respectively. In control, a single action potential was evoked by the depolarizing current pulse (Fig. 12A, top). The action potential emerged from a subthreshold oscillation (not illustrated). Mathematical reduction of the maximum conduc-

tance of  $I_{TOC-S}$  by 60–90% (to mimic the inactivation of  $I_{TOC-S}$  by depolarization to near –50 mV in vitro) caused a transient spike burst to emerge in response to the same stimulus (Fig. 12B, top). In general, the duration of the transient spike burst was correlated with the degree of reduction of  $I_{TOC-S}$ . The ionic mechanism of this change in discharge properties is clarified by examination of the dynamic interaction of  $I_{4-AP}$  and  $I_{TOC-S}$  (Fig. 12, A and B, middle). After the spike in control, both currents are activated on the rebound of the afterhyperpolarization and  $I_{TOC-S}$  decays thereafter (Fig. 12A, middle). Yet, even when  $I_{TOC-S}$  has declined in control,  $I_{4-AP}$ , which is sustained, is sufficient to prevent further active responses. However, when  $I_{TOC-S}$  is reduced before the first action potential as in Fig. 12B,  $I_{4-AP}$  alone is not sufficient within the first ~100 ms to prevent the emergence of multiple action potentials. Ultimately,  $I_{4-AP}$  is able to overcome the depolarizing influence of  $I_{Na}$  (shown in the bottom traces of Fig. 12, A–C) and prevent sustained firing of action potentials. Therefore the contribution of  $I_{TOC-S}$  is essential to prevent multiple spikes at the onset of a stimulus, but is not necessary to prevent sustained discharge. Thus  $I_{4-AP}$  is responsible for accommodation.

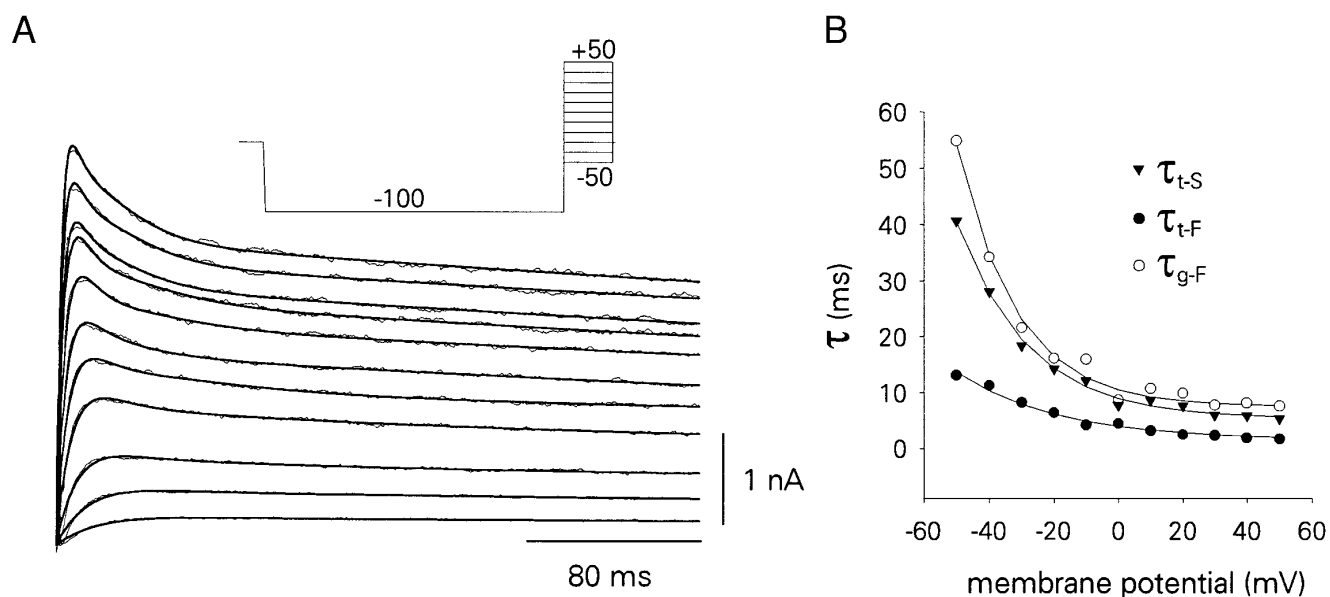


FIG. 10. Kinetic reconstruction of TOCs. *A*: current records in  $0.5 \mu\text{M}$  TTX,  $100 \mu\text{M}$   $\text{Cd}^{2+}$ ,  $20 \text{ mM}$  TEA, and  $3 \text{ mM}$   $\text{Cs}^+$  (rough traces) evoked by the voltage protocol (*inset*). Reconstructed currents are shown overlaying the data (smooth traces). *B*: voltage-dependent time constants for slow and fast activation ( $\tau_{t-S}$ ,  $\tau_{t-F}$ ) and fast inactivation ( $\tau_{g-F}$ ) plotted vs. command. Voltage-independent slow time constant ( $\tau_{g-S}$ ) not shown ( $\sim 500 \text{ ms}$ ).

Reduction of  $I_{4-AP}$  by 90–95% in the model reproduced the sustained firing behavior that characterized low doses of 4-AP applied *in vitro*. During simulated 4-AP (Fig. 12C),  $I_{\text{TOC-S}}$  is the primary outward current evoked negative to threshold and acts to repolarize the  $V_M$ . At first glance, in the records for  $I_{\text{TOC-S}}$  in Fig. 12C, *middle*, it appears that the

magnitude of  $I_{\text{TOC-S}}$  is as large as, if not larger than, the magnitude of  $I_{4-AP}$  under reduced  $I_{\text{TOC-S}}$  conditions, which was sufficient to prevent sustained discharge (Fig. 12B, *middle*).  $I_{\text{TOC-S}}$  is not able to terminate the spiking in reduced  $I_{4-AP}$  conditions because of slow kinetics. The interspike activation of  $I_{\text{TOC-S}}$  is slower than that of  $I_{4-AP}$  (compare the

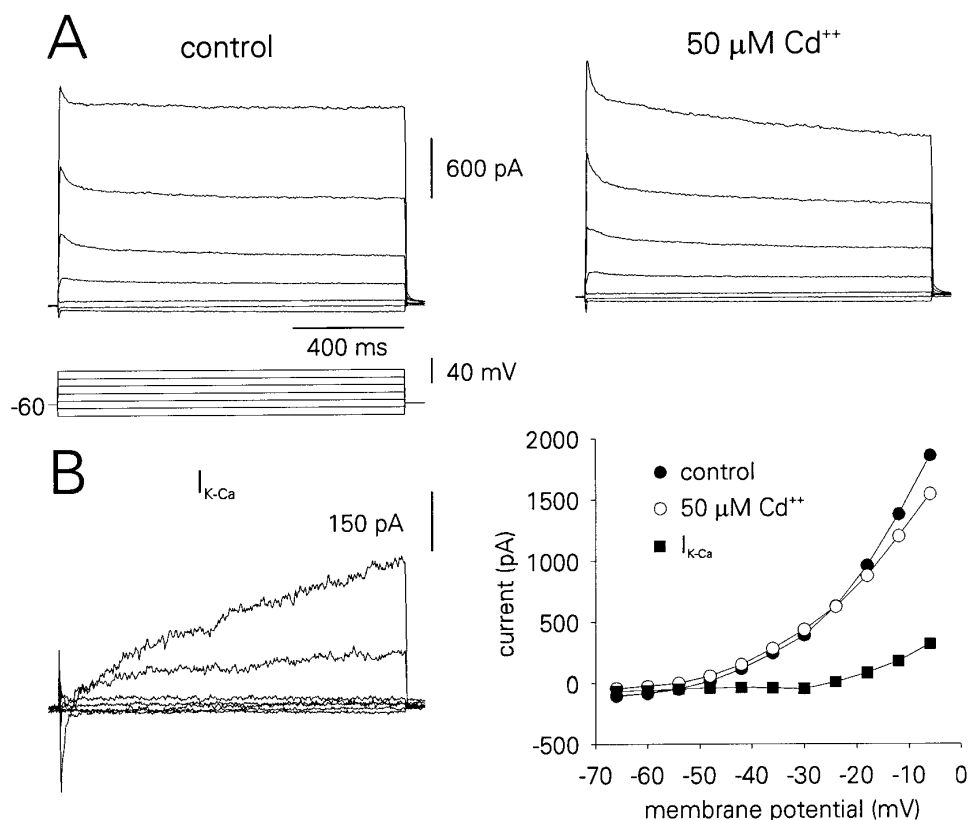


FIG. 11. Isolation of the  $\text{Ca}^{2+}$ -dependent  $\text{K}^+$  current  $I_{\text{K-Ca}}$  in Mes 5. *A*: outward currents evoked by command potentials (*bottom*) from  $-60 \text{ mV}$  in  $0.5 \mu\text{M}$  TTX (*left*) and after application of  $50 \mu\text{M}$   $\text{Cd}^{2+}$  (*right*). *B*:  $I_{\text{K-Ca}}$  (*left*) obtained by subtraction of  $\text{Cd}^{2+}$  from *A* and plotted vs. command potential on the quasi-steady-state current-voltage curve (*right*,  $\blacksquare$ ). Control and  $\text{Cd}^{2+}$  currents from *A* are also illustrated on the current-voltage curve ( $\bullet$  and  $\circ$ , respectively).

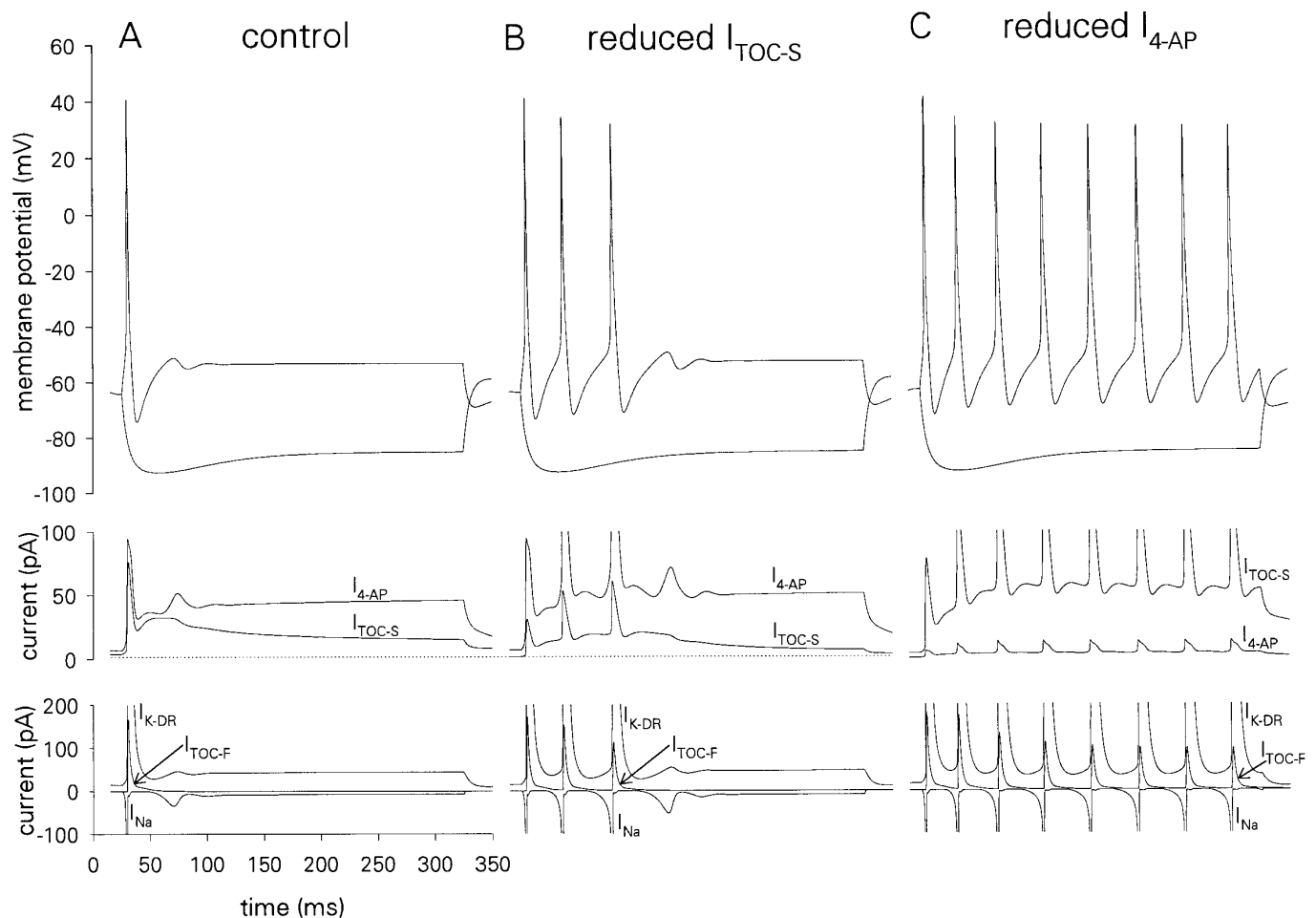


FIG. 12. Modeling results. *Top traces* in A–C: membrane potential responses to  $-110$ - and  $+100$ -pA simulated current injections. *Middle traces*: dynamic interaction of  $I_{TOC-S}$  and  $I_{4-AP}$  during the model responses as illustrated above. *Bottom traces*:  $Na^+$  current ( $I_{Na}$ ),  $I_{K-DR}$ , and  $I_{TOC-F}$ . In all traces of membrane potential, the response to hyperpolarizing current was nearly identical. A: in control, a single action potential was evoked that accommodated rapidly in a damped oscillation. Calibrations apply to A–C. B:  $I_{TOC-S}$  was reduced by 60%, causing the emergence of a spike burst before rapid activation of  $I_{4-AP}$  (note repolarizing hump following the 3rd action potential) terminates the response. C:  $I_{4-AP}$  was reduced by 93% to simulate 4-AP application, resulting in sustained repetitive spiking. Although  $I_{TOC-S}$  is activated to a great extent, its kinetics is not rapid enough during the interspike interval to terminate the nascent action potentials caused by  $Na^+$  current.

repolarizing humps of the currents between B and C, *middle*). The ability of  $I_{4-AP}$  to activate more rapidly in response to depolarization is especially clear in Fig. 12B, *middle*, where, as the membrane begins to form a fourth spike,  $I_{4-AP}$  shows a particularly rapid peak of activity that prevents spike initiation.  $I_{TOC-S}$ , on the other hand, in reduced  $I_{4-AP}$  conditions (Fig. 12C, *middle*) is not able to peak as quickly until action potentials occur (note the slower repolarizing humps of  $I_{TOC-S}$  in Fig. 12C, *middle*, followed by larger responses during spikes). Therefore  $I_{4-AP}$  is the critical factor whose removal causes Mes 5 sensory cells to move from quiescent neurons whose discharge accommodates to neurons that can discharge repetitively.

We can infer from the model that  $I_{Na}$ ,  $I_{TOC-F}$ , and  $I_{K-DR}$  primarily govern the characteristics of the single action potential. Whether the cell showed single or repetitive spikes, these three currents behaved similarly during the course of individual spikes (compare the similar shapes of current traces in Fig. 12, A–C, *bottom*).

The model did not replicate the repolarizing notch phe-

nomenon (Fig. 1B, *left*). Plateaulike action potentials, however, were reproduced by the model as maximum  $Ca^{2+}$  conductances were adjusted and the delayed rectifier current was reduced 80–85% (not shown).

## DISCUSSION

The intrinsic membrane properties of Mes 5 neurons are responsible for shaping the electrical output of the peripheral sensory endings, somata, and central synaptic terminals of these cells. Our conclusions regarding the functional properties of these intrinsic membrane properties have been reached on the basis of physiological and theoretical data. An inevitable limitation derives from the use of neonatal animals: there are no data currently available regarding developmental changes in Mes 5. The use of juvenile or adult animals was prevented by the difficulties associated with voltage clamping large neurons with low  $R_{NS}$  and the low visual resolution of rat brain stem tissue after 6 days.

### Role of $I_{4-AP}$

4-AP application in Mes 5 unmasked a sustained outward current ( $I_{4-AP}$ ), active at rest, that exerts a substantial degree of control over the excitable properties of Mes 5. Accommodation was abolished during application of 4-AP in doses sufficient to block  $I_{4-AP}$  (50–100  $\mu\text{M}$ ) but not sufficient to block  $I_{\text{TOC-S}}$  (>500  $\mu\text{M}$ ). In fact, during 4-AP application cells often became spontaneously active at  $V_{\text{MS}}$  positive to  $-55$  mV (Fig. 1B, right). The change in spiking behavior under 4-AP is attributed to 1) the voltage range in which  $I_{4-AP}$  operates ( $-60$  to  $-30$  mV) and 2) its sustained kinetics. Although active at rest,  $I_{4-AP}$  will be recruited further by any depolarizing stimulus attempting to raise the cell to threshold (approximately  $-45$  mV). Moreover, its activation will occur rapidly on the basis of the rapid phase of its kinetics. These properties of  $I_{4-AP}$  were demonstrated in the model, because the current showed rapid recruitment during membrane depolarization (see especially Fig. 12B, middle), and ultimately produced accommodation. Although  $I_{\text{TOC-S}}$  is active in the subthreshold voltage range, its kinetics is too slow to prevent spike discharge (see Fig. 12C, middle). As a target for neuromodulation, pathological modification, or differential genetic expression,  $I_{4-AP}$  represents the ideal candidate for changing the “mode” of Mes 5 from largely quiescent to excitable.

Puil et al. (1989) and Stansfeld et al. (1986) have identified 4-AP-sensitive, slowly inactivating outward currents whose block caused trigeminal root ganglia and visceral sensory neurons to discharge sustained repetitive spike trains in response to current stimuli that previously evoked only single action potentials.  $I_{4-AP}$  in Mes 5 is a sustained current, in contrast to the 4-AP-sensitive currents identified by the aforementioned investigators, which showed slow inactivation. One possible explanation for the inconsistencies regarding kinetic properties of 4-AP-sensitive currents may be explained if, like Mes 5, more than one 4-AP-sensitive outward current is evoked in trigeminal root ganglia and visceral sensory cells. Steady-state inactivation of  $I_{\text{TOC-S}}$  (at  $-40$  mV) was essential to separate this transient 4-AP-sensitive current from  $I_{4-AP}$  in Mes 5 because the two currents had very similar activation profiles in the range from  $-60$  to  $-30$  mV (Figs. 4 and 9). TOCs of dorsal root ganglia can be substantially deinactivated at resting potential in solutions containing normal concentrations of divalent cations and only fully inactivate at  $\sim 0$  mV (see Fig. 3 and 5 of Gold et al. 1996). Therefore it seems possible that the 4-AP-sensitive currents of Puil et al. (1989) and Stansfeld et al. (1986) could represent composite currents consisting of distinct transient and sustained components that we were able to distinguish in Mes 5. An alternative explanation could emanate from the kinetic heterogeneity of  $\text{K}^+$  channels that share similar pharmacology (Grissmer et al. 1994).

4-AP-sensitive ion channels in mammalian sensory neurons have been localized to peripheral endings (Kirchhoff 1992), axons (Bowe et al. 1987; Kocsis et al. 1986, 1987), and somata (Puil et al. 1989; Spigelman and Puil 1989; Stansfeld et al. 1986). Pharmacological blockade of these channels causes repetitive burstlike discharge at all sites. Distinctly different responses are seen in the axons (Kocsis et al. 1986) of motoneurons. Caution must be exercised in

generalizing our results to the morphological structures of a single sensory neuron, or sensory neurons in general, given the heterogeneity of pharmacological and kinetic properties of  $\text{K}^+$  channels and their subcellular distribution. Nevertheless, the evidence suggests that sensory neurons in particular are endowed with 4-AP-sensitive channels (which are analogous to  $I_{4-AP}$ ) whose block elicits burstlike discharge. The properties of these channels have clinical relevance because 4-AP has been shown to restore conduction to acutely demyelinated sensory fibers (Targ and Kocsis 1985) and chronically lesioned fibers (Blight 1989). Moreover, treatment of spinal cord injuries has benefited from the restorative effects of aminopyridines on damaged axons (Hansebout et al. 1993; Waxman 1993).

### Role of $I_{\text{K-DR}}$

A sustained TEA-sensitive current was identified in Mes 5 and called  $I_{\text{K-DR}}$  because it was similar to delayed-rectifier-type currents documented in sympathetic and sensory neurons (Galvan and Sedlmeir 1984; Kostyuk et al. 1981a; Vanner et al. 1993; Wang and McKinnon 1995). Although this current was on average 7 times the magnitude of  $I_{4-AP}$  at full activation, its removal by pharmacological block did not normally cause repetitive spiking to occur. Its voltage dependence of activation explains this characteristic:  $I_{\text{K-DR}}$  activates at potentials greater than  $-40$  mV, which is more positive than spike threshold. Therefore, as illustrated in the model neuron,  $I_{\text{K-DR}}$  is only evoked after passing threshold during the upswing of the action potential.

TEA application in current clamp caused broadened action potentials and  $\text{Ca}^{2+}$ -mediated plateau potentials to emerge. Repolarization of both action potentials and  $\text{Ca}^{2+}$  plateau potentials occurs at very depolarized  $V_{\text{MS}}$  (greater than  $-30$  mV), which are above the activation threshold for  $I_{\text{K-DR}}$ . Block of this current by TEA would therefore cause these phenomena to emerge rather than repetitive firing. The model reproduced plateau-like action potentials of variable duration when the maximum conductance of  $I_{\text{K-DR}}$  was reduced by 85% and the level of  $\text{Ca}^{2+}$  conductance was manipulated. These results were not illustrated because 1) not every cell showed plateau responses in TEA, and 2) we did not derive the equations for our  $\text{Ca}^{2+}$  currents.

### Role of TOCs

Two distinct TOCs were identified in Mes 5 neurons ( $I_{\text{TOC-F}}$  and  $I_{\text{TOC-S}}$ ).  $I_{\text{TOC-F}}$  activates rapidly (2–14 ms) at more depolarized levels (greater than  $-40$  mV), inactivates within 8–55 ms, and is insensitive to block by 4-AP.  $I_{\text{TOC-S}}$  activates more slowly (6–41 ms) at more negative potentials (greater than  $-60$  mV), inactivates independently of voltage ( $\sim 0.5$  s), and is blocked by 4-AP at  $>500$   $\mu\text{M}$ .

In current clamp, the duration of spike trains differed as a function of  $V_{\text{M}}$ . These responses must be understood in the context of the voltage- and time-dependent properties of  $I_{\text{TOC-S}}$  and  $I_{\text{TOC-F}}$  that deinactivate as  $V_{\text{M}}$  becomes hyperpolarized.

In many systems that express fast TOCs, the membrane voltage response from hyperpolarized levels consists of a repolarizing voltage notch that delays the onset of the first

spike (Hsiao and Chandler 1995; Jahnsen and Llinas 1984; Segal et al. 1984). This phenomenon was not observed in the present study when cells were depolarized from around  $\pm 65$  mV in control conditions. This may be the result of a relatively high rheobase, which was necessary to overcome  $I_{4-AP}$  and evoke an action potential. In this scenario the relative contribution of  $I_{TOC-F}$  would be diminished by large suprathreshold stimulus currents required to overcome the repolarizing currents  $I_{4-AP}$  and  $I_{TOC-S}$ . We did observe a transient repolarizing notch in some cells when  $I_{TOC-S}$  and  $I_{4-AP}$  were attenuated by 4-AP application. Under these conditions the block of the 4-AP-sensitive currents enhances the relative contribution of  $I_{TOC-F}$  (not blocked), which is then able to elicit a notchlike repolarization before its contribution declines (because of inactivation) and spiking commences. The model did not reproduce the notch effect.

After the first evoked spike from hyperpolarized levels, subsequent action potentials are prevented by the contribution of  $I_{TOC-S}$  and  $I_{4-AP}$ . On the basis of the model simulations,  $I_{TOC-S}$  is active in the voltage range near threshold, rises substantially during the course of an action potential, and exhibits a period of significant activation lasting  $\sim 40$  ms. Thereafter it declines because of inactivation (Fig. 12A, *middle*).  $I_{TOC-S}$  is, therefore, critical during the period following the first spike when the membrane voltage response begins to form a subsequent spike. If  $I_{TOC-S}$  is not present, the contribution of  $I_{4-AP}$  is not sufficient to prevent a volley of several spikes, although in the end  $I_{4-AP}$  is sufficient to produce accommodation (Fig. 1A or 12B, *top*). The inactivation properties of  $I_{TOC-S}$  show that at  $-62$  mV the current is 50% deactivated. Therefore modulation of the resting potential can affect the integrative properties of the cell.

Millimolar concentrations of divalent cations such as  $Cd^{2+}$  produce shifts in the voltage dependence of TOCs (Davidson and Kehl 1995; Mayer and Sugiyama 1988) that can confound characterization and functional interpretation of their properties. On the basis of the quantitative data of Mayer and Sugiyama (1988) in dorsal root ganglia,  $50 \mu M Mn^{2+}$  would positively shift the voltage dependence of activation by 0.14 mV and that of inactivation by 0.27 mV. The authors point out that  $Cd^{2+}$  is more effective in shifting voltage dependence, but even if  $Cd^{2+}$  is 10 times as efficacious, any shift would still be  $\leq 2.7$  mV, which is unlikely.

### Functional implications

Mes 5 neurons are unique among sensory neurons because they are located in the CNS and receive synaptic contacts on their somata (Alley 1973; Liem et al. 1992; Luo and Dessem 1995). Consequently, Mes 5 neurons can function as typical sensory neurons or potentially as integrative interneurons (Roberts and Witkovsky 1975). Proprioceptive sensory cell bodies (located in dorsal root ganglia) accommodate in response to current injection (Nowycky 1992), similar to a low-pass filter that reflects axonal activity but does not contribute to orthodromic flow. Interneurons, conversely, integrate synaptic signals at their soma-axon hillock to produce orthodromic impulses. Mes 5 would normally be expected to accommodate in response to excitatory synaptic input unless critical outward currents such as  $I_{4-AP}$  were altered by neuromodulators or in response to disease. Patholo-

gies such as myofascial pain syndromes, tardive dyskinesia, or nocturnal bruxisms are conditions that could be generated by abnormal somatic spike genesis or ectopic discharge.

The present study provides the first detailed biophysical data and model for the control of Mes 5 neurons by 4-AP and TEA-sensitive outward currents. From this we can begin to make realistic predictions as to the effects of neuromesengers on the excitability of these neurons at peripheral, axonal, and central locations. It is precisely this approach that we believe will be necessary to ultimately understand the function of the various neurons that make up the circuits responsible for oral-motor pattern generation.

### APPENDIX

This section details the equations and parameters utilized in the simulations of Mes 5 neurons.

#### Numerical reconstruction of voltage-dependent currents

Voltage-clamp data were fit to kinetic current according to modified HH-type equations (Hodgkin and Huxley 1952)

$$I_X(V,t) = g_{X-MAX} m^p(V,t) h^q(V,t) (V_M - E_X)$$

where  $I_X$  is the current carried by ion  $X$  and  $g_{X-MAX}$  is its maximal whole cell conductance;  $m$  and  $h$  are voltage- and time-dependent gating variables for activation and inactivation, respectively. Gating variables are raised to integer exponents ( $p$ ,  $q$ ).  $V_M$  is the membrane potential and  $E_X$  is the Nernst potential for ion  $X$ .

Gating variable dynamics were modeled as the solution to the first-order ordinary differential equation (ODE)

$$dm/dt = (m_\infty - m)/\tau_m$$

where  $m_\infty$  represents the steady-state value of  $m$  derived from the voltage dependence of activation (or inactivation) and  $\tau_m$  was empirically derived. The voltage dependence of activation or inactivation for all currents was a sigmoidal relation of the form

$$g/g_{MAX} \text{ or } I/I_{MAX} = \{1 + \exp[(V_M - V_{1/2-MAX})/k]\}^{-1}$$

where  $g/g_{MAX}$  or  $I/I_{MAX}$  is the normalized conductance or current at the command potential  $V_M$ ,  $V_{1/2-MAX}$  is the voltage of half-maximal activation, and  $k$  is the negative reciprocal slope at  $V_{1/2-MAX}$ . Mathematical expressions were developed for time constants ( $\tau$ ) of each gating variable as  $f(V_M)$ .

We utilized these methods to reconstruct the  $K^+$  currents ( $I_{4-AP}$ ,  $I_{K-DR}$ ,  $I_{K-Ca}$ ,  $I_{TOC-F}$ , and  $I_{TOC-S}$ ) and mixed cationic current ( $I_h$ ) (not displayed). Fast  $Na^+$  current ( $I_{Na}$ ) was adapted from sympathetic ganglion cells (Belluzzi and Sacchi 1991).  $Ca^{2+}$  currents ( $I_{CaN}$ ,  $I_{CaT}$ ) were adapted from nodose sensory neurons (Schild et al. 1994).

#### $V_M$

$V_M$  trajectory was described as the solution to the first-order ODE

$$dV_M/dt = -(I_{Na} + I_{CaN} + I_{CaT} + I_{4-AP} + I_{K-DR} + I_{TOC} + I_h + I_{LEAK} + I_{K-Ca} - I_{STIM})/C_M$$

#### Inward currents

$I_{Na}$ : TTX-SENSITIVE  $Na^+$  CURRENT

$$I_{Na} = g_{Na-MAX} m^3 h (V_M - E_{Na})$$

$$dm/dt = (m_\infty - m)/\tau_m$$

$$m_\infty = \{1.0 + \exp[(V_M + 36.0)/-7.2]\}^{-1}$$

$$\tau_m = 0.06 + [63.0 \exp(0.04V_M) + 0.923 \exp(-0.03351V_M)]^{-1}$$

$$dh/dt = (h_\infty - h)/\tau_h$$

$$h_\infty = \{1.0 + \exp[(V_M + 65.0)/6.5]\}^{-1}$$

$$\tau_h = 40(\{1.0 + \exp[(V_M + 10.0)/4.5]\}^{-1} + \{1.0 + \exp[(V_M + 60.0)/-10.0]\}^{-1}) - 39.9$$

$I_h$ : HYPERPOLARIZATION-ACTIVATED MIXED CATIONIC CURRENT

$$I_h = g_{h-MAX}[bq_1^3 + (1 - b)q_2^3](V_M - E_h)$$

$$dq_1/dt = (q_{1\infty} - q_1)/\tau_{qFAST}$$

$$dq_2/dt = (q_{2\infty} - q_2)/\tau_{qSLOW}$$

$$q_{1\infty} = q_{2\infty} = \{1 + \exp[(V_M + 90.16)/7.3]\}^{-1}$$

$$\tau_{qFAST} = 105.0 \exp[-(0.031)^2(V_M + 90.0)^2] + 11.0$$

$$\tau_{qSLOW} = 445.0 \exp[-(0.031)^2(V_M + 90.0)^2] + 68.0$$

$I_{CaN}$ : HIGH-THRESHOLD  $Ca^{2+}$  CURRENT

$$I_{CaN} = g_{CaN-MAX}d_N(0.55f_{N1} + 0.45f_{N2})(V_M - E_{Ca})$$

$$dd_N/dt = (d_{N\infty} - d_N)/\tau_{dN}$$

$$d_{N\infty} = \{1.0 + \exp[(V_M + 20.0)/-4.5]\}^{-1}$$

$$\tau_{dN} = 3.25 \exp[-0.00176(V_M + 31.0)^2] + 0.395$$

$$df_{N1}/dt = (f_{N1\infty} - f_{N1})/\tau_{fN1}$$

$$df_{N2}/dt = (f_{N2\infty} - f_{N2})/\tau_{fN2}$$

$$f_{N1\infty} = \{1.0 + \exp[(V_M + 20.0)/25.0]\}^{-1}$$

$$f_{N2\infty} = \{1.0 + \exp[(V_M + 40.0)/10.0]\}^{-1} + 0.2\{1.0 + \exp[(V_M + 5.0)/-10.0]\}^{-1}$$

$$\tau_{fN1} = 33.5 \exp[-0.00156(V_M + 30.0)^2] + 5.0$$

$$\tau_{fN2} = 225.0 \exp[-0.000756(V_M + 40.0)^2] + 75.0$$

$I_{CaT}$ : LOW-THRESHOLD  $Ca^{2+}$  CURRENT

$$I_{CaT} = g_{CaT-MAX}d_Tf_T(V_M - E_{Ca})$$

$$dd_T/dt = (d_{T\infty} - d_T)/\tau_{dT}$$

$$d_{T\infty} = \{1.0 + \exp[(V_M + 54.0)/-5.75]\}^{-1}$$

$$\tau_{dT} = 22.0 \exp[-0.0027(V_M + 68.0)^2] + 2.5$$

$$df_T/dt = (f_{T\infty} - f_T)/\tau_{fT}$$

$$f_{T\infty} = \{1.0 + \exp[(V_M + 68.0)/6.0]\}^{-1}$$

$$\tau_{fT} = 103.0 \exp[-0.0025(V_M + 58.0)^2] + 12.5$$

*Outward currents*

$I_{4-AP}$ : 4-AP-SENSITIVE SUSTAINED CURRENT

$$I_{4-AP} = g_{4-AP-MAX}[an_1 + (1 - a)n_2](V_M - E_K)$$

$$dn_1/dt = (n_{1\infty} - n_1)/\tau_{nFAST}$$

$$dn_2/dt = (n_{2\infty} - n_2)/\tau_{nSLOW}$$

$$n_{1\infty} = n_{2\infty} = \{1 + \exp[(V_M + 48.0)/-3.9]\}^{-1}$$

$$\tau_{nFAST} = 60.0\{1 + \exp[(V_M + 55.0)/3.0]\}^{-1} + 10.0$$

$$\tau_{nSLOW} = 2700.0 \exp[-(0.088)^2(V_M + 62.0)^2] + 50.0$$

$I_{K-DR}$ : TEA-SENSITIVE SUSTAINED CURRENT

$$I_{K-DR} = g_{K-DR-MAX}p(V_M - E_K)$$

$$dp/dt = (p_\infty - p)/\tau_p$$

$$p_\infty = \{1 + \exp[(V_M + 4.2)/-12.9]\}^{-1}$$

$$\tau_p = 25.0(\{1.0 + \exp[(V_M + 40.0)/-15.0]\}^{-1} + \{1.0 + \exp[(V_M - 25.0)/2.0]\}^{-1}) - 23.0$$

$I_{TOC}$ : TOCs

$$I_{TOC} = I_{TOC-S} + I_{TOC-F}$$

$$I_{TOC-S} = g_{TOC-S-MAX}t_Sg_S(V_M - E_K)$$

$$I_{TOC-F} = g_{TOC-F-MAX}(t_F)^3g_F(V_M - E_K)$$

$$dt_S/dt = (t_{S\infty} - t_S)/\tau_{tS}$$

$$dt_F/dt = (t_{F\infty} - t_F)/\tau_{tF}$$

$$t_{S\infty} = \{1.0 + \exp[(V_M + 37.23)/-7.7]\}^{-1}$$

$$t_{F\infty} = \{1.0 + \exp[(V_M - 5.0)/-14.95]\}^{-1}$$

$$\tau_{tS} = 76.0 \exp[-(V_M + 66.86)/21.94] + 5.3$$

$$\tau_{tF} = 15.15 \exp[-(V_M + 56.74)/30.97] + 1.5$$

$$dg_S/dt = (g_{S\infty} - g_S)/\tau_{gS}$$

$$dg_F/dt = (g_{F\infty} - g_F)/\tau_{gF}$$

$$g_{S\infty} = g_{F\infty} = \{1.0 + \exp[(V_M + 62.73)/8.87]\}^{-1}$$

$$\tau_{gF} = 90.37 \exp[-(V_M + 61.87)/18.11] + 7.5$$

$$\tau_{gS} = 500.0 \text{ ms}$$

$I_{K-Ca}$ :  $Ca^{2+}$ -DEPENDENT  $K^+$  CURRENT

$$I_{K-Ca} = g_{K-Ca-MAX}k(V_M - E_K)$$

$$dk/dt = (k_\infty - k)/\tau_k$$

$$k_\infty = \{1 + \exp[(V_M + 15.0)/-4.0]\}^{-1}$$

$$\tau_k = 250.0 \exp[-0.0025(V_M + 15.0)^2] + 100.0$$

*Other currents*

$I_{LEAK}$ : LEAKAGE CURRENT

$$I_{LEAK} = g_{LEAK}(V_M - E_{LEAK})$$

$I_{STIM}$  = step function of variable magnitude and duration

*Ca<sup>2+</sup> balance*

$Ca^{2+}$  concentration dynamics were modeled for an intracellular compartment representing 70% of the cell volume (allowing 30% for intracellular organelles), a 1- $\mu$ M shell surrounding the neuron, a sequestering buffer in the cytosol, and an external bathing medium.  $Ca^{2+}$  flux between compartments was driven by diffusion between the bathing medium and the perineuronal shell, ionic currents across the membrane, and intracellular buffering.

Intracellular  $Ca^{2+}$  dynamics were governed by ionic current flux and intracellular buffering by ethylene glycol-bis( $\beta$ -aminoethyl ether)- $N,N,N',N'$ -tetraacetic acid (EGTA) (from the pipette solution) according to the ODE

$$d[Ca^{2+}]_i/dt$$

$$= -(I_{CaT} + I_{CaN})/(z_{Ca}V_iF) - k_f[Ca^{2+}]_i[EGTA] + k_b[Ca-EGTA]$$

The first term in the differential equation represents the contribution of ionic current flux [amperes converted to concentration

change by valence ( $z_{Ca}$ ), an intracellular volume ( $V_i$ ) of 0.00644 nl, and Faraday's constant ( $F$ )]. The second and third terms represent first-order kinetic binding to EGTA with forward and backward rate constants ( $k_f$ ,  $k_b$ ) that were determined on the basis of the dissociation constant for EGTA ( $\log K = 10.86$ ) and an estimate of the forward rate constant ( $\log k_f = 8.0$ ).

Perineuronal shell  $[Ca^{2+}]_e$  dynamics resulted from diffusion and ionic currents according to the ODE

$$d[Ca^{2+}]_e/dt = ([Ca^{2+}]_o - [Ca^{2+}]_e)/\tau_{Ca} + (I_{CaT} + I_{CaN})/(z_{Ca}V_eF)$$

The first term accounts for diffusion along a  $Ca^{2+}$  concentration gradient between the bathing medium and the perineuronal shell.  $\tau_{Ca}$  is the slow time constant for this process derived for the surface area of the shell considering the diffusion rate of  $Ca^{2+}$  in aqueous medium ( $6.0 \times 10^{-6} \text{ cm}^2/\text{s}$ ). The second term represents the contribution of ionic current flux similar to that employed in the intracellular  $Ca^{2+}$  differential equation but with opposite sign and shell volume ( $V_e$ ) of 0.00229 nl. The reversal potential for  $Ca^{2+}$  was updated dynamically by the Nernst equation.

The solutions to the ODEs below describe the trajectory of bound and unbound intracellular buffer

$$d[EGTA]/dt = k_b[Ca-EGTA] - k_f[Ca^{2+}]_i[EGTA]$$

$$d[Ca-EGTA]/dt = k_f[Ca^{2+}]_i[EGTA] - k_b[Ca-EGTA]$$

### Parameters

$a = 0.5$   
 $b = -0.01V_M - 0.24$   
 $[Ca^{2+}]_o = 2.0 \text{ mM}$   
 $C_M = 21.0 \text{ pF}$   
 $E_{Ca} = [(RT)/(z_{Ca}F)] \ln([Ca^{2+}]_e/[Ca^{2+}]_i)$   
 $E_{Na} = 50.0 \text{ mV}$   
 $E_h = -34.8 \text{ mV}$   
 $E_K = -97.0 \text{ mV}$   
 $E_{LEAK} = -56.0 \text{ mV}$   
 $F = 96500.0 \text{ C/mol}$   
 $g_{4-AP-MAX} = 8.3 \text{ nS}$   
 $g_{CaN-MAX} = 3.0 \text{ nS}$   
 $g_{CaT-MAX} = 0.35 \text{ nS}$   
 $g_{h-MAX} = 20.2 \text{ nS}$   
 $g_{K-DR-MAX} = 45.0 \text{ nS}$   
 $g_{K-Ca-MAX} = 4.0 \text{ nS}$   
 $g_{LEAK-MAX} = 3.0 \text{ nS}$   
 $g_{Na-MAX} = 901.0 \text{ nS}$   
 $g_{TOC-MAX-S} = 5.0 \text{ nS}$   
 $g_{TOC-MAX-F} = 180.0 \text{ nS}$   
 $k_b = 1.4 \times 10^{-6} \text{ ms}^{-1}$   
 $k_f = 100 \text{ ms}^{-1} \text{ mM}^{-1}$   
 $R = 8314.0 \text{ J} \cdot \text{kg}^{-1} \cdot \text{mol}^{-1} \cdot \text{K}^{-1}$   
 $T = 298 \text{ K}$   
 $\tau_{Ca} = 4100.0 \text{ ms}$   
 $V_e = 0.00229 \text{ nl}$   
 $V_i = 0.00644 \text{ nl}$   
 $z_{Ca} = 2.0$

We thank Drs. A. Berger, D. Bayliss, and M. Umeiya for generous assistance with development of the thin brain slice patch-clamp technique for trigeminal neurons. We also thank Dr. Alan Garfinkel for assistance with assembling and evaluating the mathematical model, and M. Z. Castillo and A. M. Lapin for technical contributions.

This work was supported by National Institute of Dental Research Grant RO1 DE-06193.

Address for reprint requests: S. H. Chandler, Dept. of Physiological Science, UCLA, 2851 Slichter Hall, Los Angeles, CA 90095-1568.

Received 22 July 1996; accepted in final form 16 October 1996.

### REFERENCES

- ADAMS, P. R., BROWN, D. A., AND CONSTANTIN, A. Pharmacological inhibition of the M-current. *J. Physiol. Lond.* 332: 223–262, 1982.
- ALLEY, K. E. Quantitative analysis of the synaptogenic period in the trigeminal mesencephalic nucleus. *Anat. Rec.* 177: 49–60, 1973.
- APPENTENG, K., CURTIS, J. C., GRIMWOOD, P. D., MIN, M.-Y., AND YANG, H.-W. Excitatory synaptic transmission in the rat trigeminal motor nucleus. In: *Brain and Oral Functions*, edited by T. Morimoto, T. Matsuya, and K. Takada. New York: Elsevier, 1995, p. 107–114.
- BELLUZZI, O. AND SACCHI, O. A five-conductance model of the action potential in the rat sympathetic neurone. *Prog. Biophys. Mol. Biol.* 55: 1–30, 1991.
- BLIGHT, A. R. Effect of 4-aminopyridine on axonal conduction-block in chronic spinal cord injury. *Brain Res. Bull.* 22: 47–52, 1989.
- BOSTOCK, H., SEARS, T. A., AND SHERRATT, R. M. The effects of 4-aminopyridine and tetraethylammonium ions on normal and demyelinated mammalian nerve fibers. *J. Physiol. Lond.* 313: 310–315, 1981.
- BOWE, C. M., KOCSIS, J. D., TARG, E. F., AND WAXMAN, S. G. Physiological effects of 4-aminopyridine on demyelinated mammalian motor and sensory fibers. *Annu. Rev. Neurol.* 22: 264–268, 1987.
- CHANDLER, S. H., HSIAO, C.-F., INOUE, T., AND GOLDBERG, L. J. Electrophysiological properties of guinea pig trigeminal motoneurons recorded in vitro. *J. Neurophysiol.* 71: 129–145, 1994.
- CORBIN, K. B. AND HARRISON, F. Function of mesencephalic root of fifth cranial nerve. *J. Neurophysiol.* 3: 424–435, 1940.
- DAVIDSON, J.-L. AND KEHL, S. J. Changes of activation and inactivation gating of the transient potassium current of rat pituitary melanotrophs caused by micromolar  $Cd^{++}$  and  $Zn^{++}$ . *Can. J. Physiol. Pharmacol.* 73: 36–42, 1995.
- DESSEM, D. AND TAYLOR, A. Morphology of jaw-muscle spindle afferents in the rat. *J. Comp. Neurol.* 282: 389–403, 1989.
- EDWARDS, F. A., KONNERTH, A., SAKMANN, B., AND TAKAHASHI, T. A thin slice preparation for patch clamp recordings from neurones of the mammalian central nervous system. *Pfluegers Arch.* 414: 600–612, 1989.
- GALVAN, M. AND SEDLMEIR, C. Outward currents in voltage clamped rat sympathetic neurones. *J. Physiol. Lond.* 356: 115–133, 1984.
- GOLD, M. S., SHUSTER, M. J., AND LEVINE, J. D. Characterization of six voltage-gated  $K^+$  currents in adult rat sensory neurons. *J. Neurophysiol.* 75: 2629–2646, 1996.
- GOLDBERG, L. J. AND CHANDLER, S. H. Central mechanisms of rhythmical trigeminal activity. In: *Neurophysiology of Jaws and Teeth*, edited by A. Taylor. New York: Macmillan, 1990, p. 268–293.
- GRISSMER, S., NGUYEN, A. N., AIYAR, J., HANSON, D. C., MATHER, R. J., GUTMAN, G. A., KARMILOWICZ, M. J., AUPERIN, D. D., AND CHANDY, K. G. Pharmacological characterization of five cloned voltage-gated  $K^+$  channels, types Kv1.1, 1.2, 1.3, 1.5, and 3.1, stably expressed in mammalian cell lines. *Mol. Pharmacol.* 45: 1227–1234, 1994.
- HANSEBOUT, R. R., BLIGHT, A. R., FAWCETT, S., AND REDDY, K. 4-Aminopyridine in chronic spinal cord injury: a controlled, double-blind, crossover study in eight patients. *J. Neurotrauma* 10: 1–18, 1993.
- HENDERSON, G., PEPPER, C. M., AND SHEFNER, S. A. Electrophysiological properties of neurons contained in the locus coeruleus and mesencephalic nucleus of trigeminal nerve in vitro. *Exp. Brain Res.* 45: 29–37, 1982.
- HODGKIN, A. L. AND HUXLEY, A. F. A quantitative description of membrane current and its application to conduction and excitation in nerve. *J. Physiol. Lond.* 117: 500–544, 1952.
- HSIAO, C.-F. AND CHANDLER, S. H. Characteristics of a fast transient outward current in guinea pig trigeminal motoneurons. *Brain Res.* 695: 217–226, 1995.
- JAHNSEN, H. AND LLINAS, R. Ionic basis for the electroresponsiveness and oscillatory properties of guinea-pig thalamic neurones in vitro. *J. Physiol. Lond.* 349: 227–247, 1984.
- JERGE, C. R. Organization and function of the trigeminal mesencephalic nucleus. *J. Neurophysiol.* 26: 393–402, 1963.
- KATAKURA, N., JIA, L., AND NAKAMURA, Y. NMDA-induced rhythmical activity in XII nerve of isolated CNS from newborn rats. *Neuroreport* 6: 601–604, 1995.
- KIRCHHOFF, C., LEAH, J. D., JUNG, S., AND REEH, P. W. Excitation of cutaneous sensory nerve endings in the rat by 4-aminopyridine and tetraethylammonium. *J. Neurophysiol.* 67: 125–131, 1992.
- KOCSIS, J. D., BOWE, C. M., AND WAXMAN, S. G. Different effects of 4-aminopyridine on sensory and motor fibers: pathogenesis and paresthesias. *Neurology* 36: 117–120, 1986.
- KOCSIS, J. D., ENG, D. L., GORDON, T. R., AND WAXMAN, S. G. Functional

- differences between 4-aminopyridine and tetraethylammonium-sensitive potassium channels in myelinated axons. *Neurosci. Lett.* 75: 193–198, 1987.
- KOGO, M., FUNK, G., AND CHANDLER, S. H. Rhythmical oral-motor activity recorded in an in vitro brainstem preparation. *Somatosens. Mot. Res.* 13: 39–48, 1996.
- KOSTYUK, P. G., VESELOVSKY, N. S., FEDULOVA, S. A., AND TSYNDRENKO, A. Y. Ionic currents in the somatic membrane of rat dorsal root ganglion neurons. III. Potassium currents. *Neuroscience* 6: 2439–2444, 1981a.
- KOSTYUK, P. G., VESELOVSKY, N. S., AND TSYNDRENKO, A. Y. Ionic currents in the somatic membrane of rat dorsal root ganglion neurons. I. Sodium currents. *Neuroscience* 6: 2423–2430, 1981b.
- LIEM, R. S. B., COPRAY, J. C. V. M., AND VAN WILLIGEN, J. D. Distribution of synaptic boutons in the mesencephalic trigeminal nucleus of the rat—a quantitative electron-microscopical study. *Acta Anat.* 143: 74–78, 1992.
- LUND, J. P. Mastication and its control by the brain stem. *Crit. Rev. Oral Biol. Med.* 2: 33–64, 1991.
- LUO, P. AND DESSEM, D. Morphological evidence for recurrent jaw-muscle spindle afferent feedback within the mesencephalic trigeminal nucleus. *Brain Res.* 710: 260–264, 1995.
- LUO, P., WONG, R., AND DESSEM, D. Projection of jaw-muscle spindle afferents to the caudal brainstem in rats demonstrated using intracellular biotinamide. *J. Comp. Neurol.* 358: 63–78, 1995.
- MAYER, M. L. AND SUGIYAMA, K. A modulatory action of divalent cations on transient outward current in cultured rat sensory neurones. *J. Physiol. Lond.* 396: 417–433, 1988.
- NAKAMURA, Y. AND KATAKURA, N. Generation of masticatory rhythm in the brainstem. *Neurosci. Res.* 23: 1–19, 1995.
- NOWYCKY, M. C. Voltage-gated ion channels in dorsal root ganglion neurons. In: *Sensory Neurons, Diversity, Development, and Plasticity*, edited by S. A. Scott. New York: Oxford Univ. Press, 1992, p. 97–115.
- PUIL, E., MIURA, R. M., AND SPIGELMAN, I. Consequences of 4-aminopyridine applications to trigeminal root ganglion neurons. *J. Neurophysiol.* 62: 810–820, 1989.
- PUIL, E. AND SPIGELMAN, I. Electrophysiological responses of trigeminal root ganglion neurons in vitro. *Neuroscience* 24: 635–646, 1988.
- ROBERTS, B. L. AND WITKOVSKY, P. A functional analysis of the mesencephalic nucleus of the fifth nerve in the selachian brain. *Proc. R. Soc. Lond. B Biol. Sci.* 190: 473–495, 1975.
- SCHILD, J. H., CLARK, J. W., HAY, M., MEDELOWITZ, M. C., ANDRESEN, M. C., AND KUNZE, D. L. A- and C-type rat nodose sensory neurons: model interpretations of dynamic discharge characteristics. *J. Neurophysiol.* 71: 2338–2358, 1994.
- SCHURR, A., WEST, C. A., AND RIGOR, B. M. Lactate-supported synaptic function in the rat hippocampal slice preparation. *Science Wash. DC* 240: 1326–1328, 1988.
- SEGAL, M., ROGAWSKI, M. A., AND BARKER, J. L. A transient potassium conductance regulates the excitability of cultured hippocampal and spinal neurons. *J. Neurosci.* 4: 604–609, 1984.
- SPIGELMAN, I. AND PUIL, E.  $K^+$ -channel blockade in trigeminal root ganglion neurons: effects on membrane outward currents. *J. Neurophysiol.* 62: 802–809, 1989.
- STANSFELD, C. E., MARSH, S. J., HALLIWELL, J. V., AND BROWN, D. A. 4-Aminopyridine and dendrotoxin induce repetitive firing in rat visceral sensory neurones by blocking a slowly inactivating outward current. *Neurosci. Lett.* 64: 299–304, 1986.
- STUART, G. J., DODT, H.-U., AND SAKMANN, B. Patch clamp recordings from the soma and dendrites of neurons in brain slices using infrared video microscopy. *Pfluegers Arch.* 423: 511–518, 1993.
- TARG, E. AND KOCSIS, J. D. 4-Aminopyridine leads to restoration of conduction in demyelinated rat sciatic nerve. *Brain Res.* 328: 358–361, 1985.
- VANNER, S., EVANS, J. R., MATSUMOTO, S. G., AND SURPRENANT, A. Potassium currents and their modulation by muscarine and substance P in neuronal cultures from adult guinea pig celiac ganglia. *J. Neurophysiol.* 69: 1632–1644, 1993.
- WANG, H.-S. AND MCKINNON, D. Potassium currents in rat prevertebral and paravertebral sympathetic neurones: control of firing properties. *J. Physiol. Lond.* 485: 319–335, 1995.
- WAXMAN, S. G. Aminopyridines and the treatment of spinal cord injury. *J. Neurotrauma* 10: 19–24, 1993.
- YAMADA, W. M., KOCH, C., AND ADAMS, P. R. Multiple channels and calcium dynamics. In: *Methods in Neuronal Modeling*, edited by C. Koch and I. Segev. Cambridge, MA: MIT Press, 1989, p. 97–133.